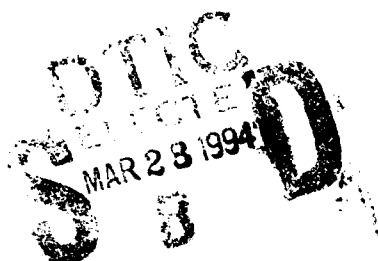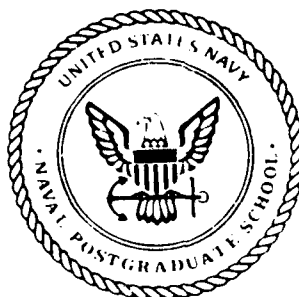# NAVAL POSTGRADUATE SCHOOL
Monterey , California

THESIS

An Analysis of Ionospheric Dayglow from
Observations of the Naval Postgraduate School
Middle Ultraviolet Spectrograph (MUSTANG)

by

Antony C. Marron

December, 1993

Thesis Advisor: David D. Cleary

Approved for public release; distibution is unlimited.

94 3 25 096

REPORT DOCUMENTATION PAGE

1. AGENCY USE ONLY (Leave blank)	2. REPORT DATE	3. REPORT TYPE AND DATES COVERED
	December 1993	Master's Thesis

4. TITLE AND SUBTITLE

An Analysis of Ionospheric Dayglow from
Observations of the Naval Postgraduate School
Middle Ultraviolet Spectrograph (MUSTANG)

5. FUNDING NUMBERS

6. AUTHOR(S)

Antony C. Marron

7. PERFORMING ORGANIZATION NAME(S) AND ADDRESS(ES)

Naval Postgraduate School
Monterey, CA 93943-5000

8. PERFORMING ORGANIZATION REPORT NUMBER

9. SPONSORING/MONITORING AGENCY NAME(S) AND ADDRESS(ES)

Naval Postgraduate School
Monterey, CA 93943-5000

10. SPONSORING/MONITORING AGENCY REPORT NUMBER

11. SUPPLEMENTARY NOTES

The views expressed in this thesis are those of the author and do not reflect
the official policy or position of the Department of Defense or the U.S. Government.

12a. DISTRIBUTION/AVAILABILITY STATEMENT

Approved for public release; distribution is unlimited.

12b. DISTRIBUTION CODE

A

13. ABSTRACT (Maximum 200 words)

Middle ultraviolet spectra of the atmospheric airglow were obtained from a March 1992 rocket flight of the NPS MUSTANG instrument. These spectra are analyzed from 1900 Å to 3100 Å, over an altitude range of 100 km to 320 km. The data are modeled with computer generated synthetic spectra for the following emissions: N2 Vegard Kaplan (VK); N2 Lyman-Birge-Hopfield (LBH); and NO Gamma (γ), Delta (δ), and Epsilon (ϵ) bands. A best fit procedure was developed. The resulting synthetic spectra agree well with obtained airglow data. Confirmation was made of the theoretical self absorption versus non-self absorption processes of the NO (0,0), (1,0), (2,0) γ resonance band emissions. NO self absorption is a necessary inclusion of any atmospheric nitric oxide analysis stratagem. Profiles of temperature versus altitude and NO column density versus altitude for the rocket flight are estimated.

14. SUBJECT TERMS			15. NUMBER OF PAGES
Airglow, Ionosphere, Ultraviolet Spectroscopy			70
			16. PRICE CODE

17. SECURITY CLASSIFICATION OF REPORT	18. SECURITY CLASSIFICATION OF THIS PAGE	19. SECURITY CLASSIFICATION OF ABSTRACT	20. LIMITATION OF ABSTRACT
Unclassified	Unclassified	Unclassified	Unlimited

**An Analysis of Ionospheric Dayglow from
Observations of the Naval Postgraduate School
Middle Ultraviolet Spectrograph (MUSTANG)**

by

Antony C. Marron
Lieutenant, United States Navy
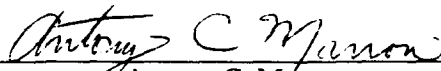B.S.(Biochemistry), San Francisco State University, 1985

Submitted in partial fulfillment of the
requirements for the degrees of

Master of Science in Applied Physics
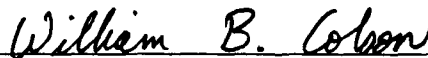
from the

NAVAL POSTGRADUATE SCHOOL
December 1993

Author: _____
Antony C. Marron

Approved by: _____
David D. Cleary, Thesis Advisor

_____
Suntharalingam Gnanalingam, Second Reader

_____
William B. Colson, Chairman
Department of Physics

ii

ABSTRACT

Middle ultraviolet spectra of the atmospheric airglow were obtained from a March 1992 rocket flight of the NPS MUSTANG instrument. These spectra are analyzed from 1900 Å to 3100 Å, over an altitude range of 100 km to 320 km. The data are modeled with computer generated synthetic spectra for the following emissions: N2 Vegard Kaplan (VK); N2 Lyman-Birge-Hopfield (LBH); and NO Gamma (γ), Delta (δ), and Epsilon (ε) bands. A best fit procedure was developed. The resulting synthetic spectra agree well with obtained airglow data. Confirmation was made of the theoretical self absorption versus non-self absorption processes of the NO (0,0), (1,0), (2,0) γ resonance band emissions. NO self absorption is a necessary inclusion of any atmospheric nitric oxide analysis stratagem. Profiles of temperature versus altitude and NO column density versus altitude for the rocket flight are estimated.

iii

TABLE OF CONTENTS

ACKNOWLEDGMENTS

This thesis could not have been completed without exceptional patience of my thesis advisor whom I also consider my friend, David D. Cleary, Ph.D.

My most special thanks to my wife Lici who has endured many evenings of my absence to finish this work. I reflect on her as a woman of uncommon beauty and of enduring friendship. I will be forever grateful.

I. INTRODUCTION

The electromagnetic properties of the earth's atmosphere are important to many areas of science such as weather forecasting, atmospheric instruments, satellite electromagnetic surveillance, and communication operations. The upper atmospheric region known as the ionosphere contains electron densities which are sufficiently high to form a plasma medium. The plasma-like properties of the ionosphere are of specific interest to the military. They strongly affect operations of systems such as high frequency (HF) radio communications, over-the-horizon radar (OTHR), ballistic missile early warning (e.g., SDI), and the Ground Wave Emergency Network (GWEN). For effective prediction of the plasma-like properties of the ionosphere an electron density profile is required.

An electron density profile is a plot of electron density versus altitude for a given time and location. In 1986, the Joint Chiefs of Staff prioritized the determination of electron density as fifth on a list of 43 critical geophysical parameters (The Joint Chiefs of Staff, 1986). The electron density varies with time (e.g., day, night, solar cycle), altitude, and geographic location. Presently, electron density profiles are determined using approximately 20 ground-based ionosonde stations worldwide. This can be very effective locally, but is inherently imprecise for a global forecasting model.

An alternative to ionosonde ground stations is to deduce density profiles of the neutral atoms and molecules in the ionosphere from naturally occuring airglow emissions. From these neutral density profiles and knowledge of atmospheric photo-chemistry one can infer electron and ion density profiles. The inference of electron densities from emission observations is

1

performed by relating measurements of natural ultraviolet emissions to the net. il species' densities.

An operational ultraviolet spectrograph that is relatively small and low-powered can easily be incorporated into an orbiting tactical communication platform or an optical surveillance satellite configuration. It would achieve continuous, passive measurements of the ultraviolet radiation emitted by the ionospheric airglow. A low earth orbit (LEO) based satellite would provide a globally complete remote sensing technique of predicting an electron density model of the Earth's ionosphere.

The Naval Research Laboratory (NRL) and The Ionospheric Physics Group at the Naval Postgraduate School (NPS) have a joint spectrographic project. The NRL project is a High Resolution Airglow and Aurora Spectrograph (HIRAAS) with an observation range of 500 Å to 1500 Å. The addition of the HIRAAS/MUSTANG experiment represents a significant progress of the global determination of electron density profiles beyond ground-based ionosondes. A sounding rocket-launched experiment was first successfully tested in March, 1990 from White Sands Missile Range, New Mexico. The data for this thesis is from the second successful launch which was conducted in March, 1992. A third rocket experiment will be conducted in March, 1994, from the Poker Flat Missile Range in Alaska. The relative high latitude of the Poker Flat Range will enable the observation of the effects of auroral electron precipitation on ionospheric photochemistry.

These sub-orbital rocket experiments will be followed by a remote sensing satellite project. The successor to the MUSTANG instrument is the Ionospheric Spectroscopy and Atmospheric Chemistry (ISAAC) instrument which is already constructed. The NPS Ionospheric Physics Group is presently calibrating ISAAC. It will be launched on the Advanced Research and Global Observation Satellite (ARGOS) in late 1995.

A. Thesis Objectives

This thesis focuses on the analysis of spectral data obtained from the March, 1992 rocket flight. The analysis extends methods used previously on subsets of the data to the observed range, 1900 Å to 3100 Å (see e.g., Cleary, 1986; Clayton, 1990; Anderson, 1990; Mack, 1991; Walden, 1991). All known emissions in this range are used in the fitting routines except OI 2972 Å, OII 2470 Å, OIII 2853 Å, and NII 2143 Å atomic lines. The result of the fitting algorithm is a set of relative scale factors as a function of altitude. The relative scale factors are converted into absolute terms and plotted against altitude. These absolute plots of intensity and column density can be used to infer an electron density profile (see e.g., McCoy, 1985; Meier, 1991).

Additional goals of this thesis are to confirm the theoretical self absorption mechanisms of the NO (0,0), (1,0), (2,0) γ band emissions, determine the NO column density profile and estimate a temperature profile for the observed altitude range.

B. Thesis Outline

This thesis is separated into seven chapters. Chapter II gives general background information on the descriptions and designations of the atmosphere and airglow emissions. A basic explanation of molecular spectra is also outlined in this section. Chapter III addresses the specific dayglow emission characteristics in the wavelength range of interest. Chapter IV presents an overview of the experiment. Chapter V gives a full breakdown of the algorithm techniques to generate a synthetic model to fit the data. Chapter VI explains the results of the study. Chapter VII concludes the document with a summary of findings and suggestions for future study. The appendices contain the plots of the final fits to the data as well as an estimated NO column density profile and atmospheric temperature profile.

3

II. BACKGROUND

A. The Atmosphere

1. General Description

T... Earth's atmosphere is designated by distinct, horizontal layers. These layers are determined by one of two primary methods. One method designates the layers based upon temperature characteristics and the other uses constituent density to classify the atmospheric boundaries. Both schemes are shown in Figure II-1 . The figure shows two temperature profiles corresponding to low and high solar activity.
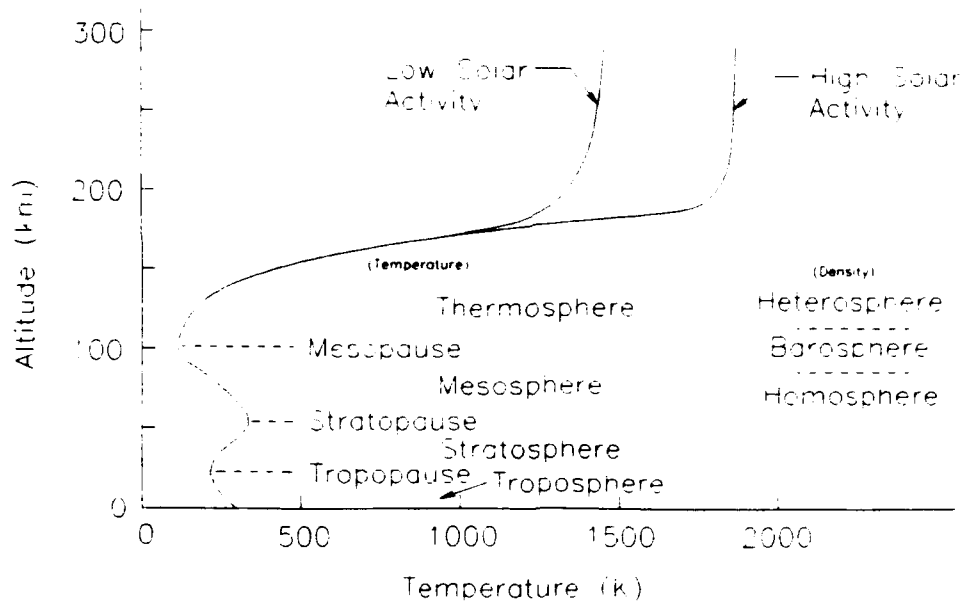
Figure II-1 Atmospheric temperature profile. Also shown are atmospheric layers designated by temperature compared with corresponding density layers.

This method of classification designates the troposphere as the region closest to the Earth's surface. In the troposphere temperature decreases with altitude, on average from about 300 K at the surface to 220 K at 10 km. The point at which temperature begins to rise is called

4

the tropopause and it determines the start of the next region, the stratosphere. The stratosphere is a relatively warm layer due to absorption of solar radiation by ozone (primarily 2000-3000 Å). The top of the stratosphere is marked by the stratopause. The next layer is labeled the mesosphere. In the mesosphere, the temperature decreases with altitude until a low of about 100 K occurs at approximately 85 km. This is the mesopause, which marks the beginning of the next layer, the thermosphere. Temperature rises steadily in the thermosphere with increasing altitude until reaching an equilibrium temperature between 1000 K and 2000 K, depending on solar activity.

Studying the atmosphere in terms of density or chemical composition gives rise to a different series of atmospheric layers. The lowest 80 kilometer layer of the atmosphere is called the homosphere. Vertical mixing of this region provides a uniform relative density ratio between various molecular species. The primary components are molecular nitrogen and oxygen and atomic argon in the well known ratio of .78: .21: .009. The remaining 0.001 is primarily helium, hydrogen, and carbon dioxide. The layer from 80 km to 100 km is designated the barosphere and it is a transition region above which very little vertical mixing occurs. Atop the barosphere is the heterosphere from 100 km to approximately 1000 km. In this area of the upper atmosphere, the relative densities vary with altitude due to differing molecular weights. The density of the atmosphere above the heterosphere is so low that individual molecule trajectories are essentially parabolic orbits. This region is labeled the exosphere.

2. The Ionosphere

The data analysis in this work pertains to the lower heterosphere. This corresponds to the ionosphere. Specifically, the first 200 km of the thermosphere where the convective mixing

5

is minimal and there exists a positive temperature gradient. The ionosphere is so designated

due to the ionization of neutral atmospheric constituents into ions and electrons. The

ionosphere is divided into four layers due to the presence of discrete electron density regions

and is depicted in Figure II-2 . The layers are labeled D, E, F_1 and F_2. The actual height and

thickness of each layer varies with solar cycle activity. The D region is the lowest layer and

typically extends from about 50 km to 90 km. The E region is from 90 km to 130 km. F_1

ordinarily exists from 130 km to 160 km during daytime periods and the F_2 region lies above

160 km.
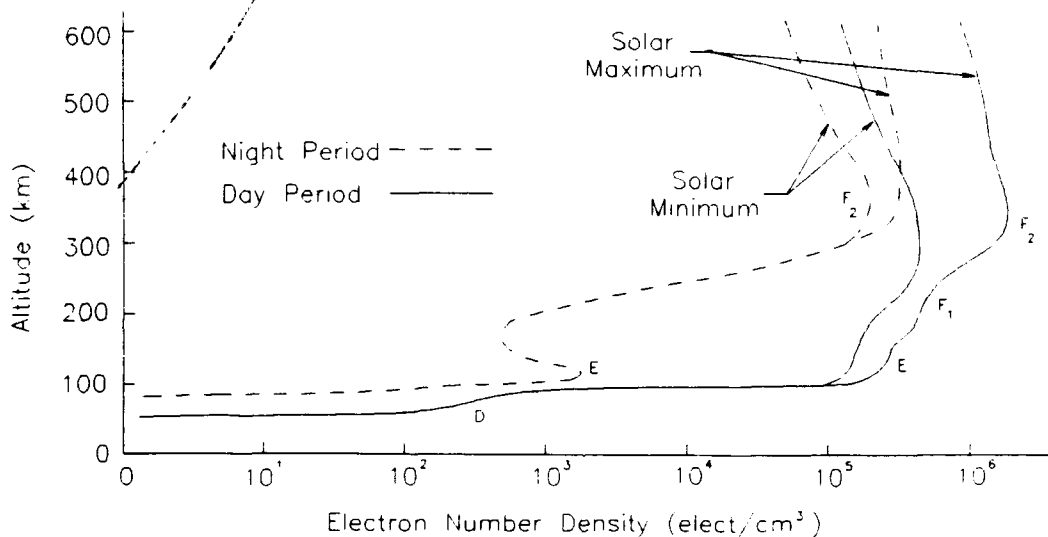
Figure II-2 Atmospheric electron density profile.

The primary mechanism for the development of the ionosphere during the daylight

hours is photo-ionization. The general chemical equation below for a single, neutral molecule

M describes this process.

$$M + h\upsilon \rightarrow M^+ + e^-$$
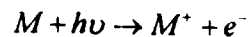
The $h\nu$ term represents solar photons with sufficient energy for ionization. The ionization rate $Q_\lambda(z)$ is proportional to: 1) the flux of photons as a function of wavelength $I_\lambda(z)$ 2) the density of neutral molecules $n(z)$ exposed to the solar flux; 3) the efficiency with which these photons cause ionization. This efficiency is termed the ionization cross-section $\sigma_i(\lambda)$. It is wavelength dependent and depends on the ionization potential of the molecule M. Thus,

$$Q_\lambda(z) = n(z) * I_\lambda(z) * \sigma_i(\lambda)$$

The photon flux decreases in intensity with decreasing altitude and the neutral species concentration decreases with increasing altitude. The product of these two quantities produces a profile with a discrete layer. This profile is referred to as a Chapman ionization profile. This is depicted in Figure II-3. In region (A) of this figure the species concentration is not high enough to cause significant photon absorption. Maximum ionization occurs at a distinct atmospheric area (B). The ionization rate falls off rapidly at lower altitudes because very few ionizing photons are able to penetrate through to the (C) section.
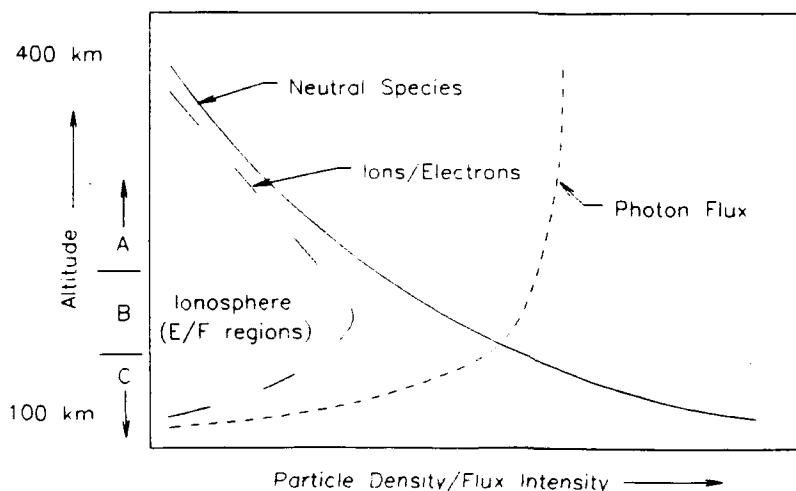
Figure II-3 Chapman Profile for ion/electron production.

Chapman (1931) was the first to provide a quantitative explanation for the formation of an atmospheric ionized layer. This ionization process is effective enough to maintain sufficient quantities of ionized species to maintain an ionospheric plasma. The collective behavior of the ionospheric plasma can affect electromagnetic waves propagating through the ionosphere and is of special interest to the military.

3. Atmospheric Airglow

The MUSTANG instrument was designed to measure emissions of the Earth's airglow. Airglow is a naturally occurring radiation from the Earth's atmosphere. Dayglow, or daytime airglow is primarily driven by photoexcitation. Also cor+ributing to dayglow are emissions from photoelectron impacts and photochemical reactions. The intensity of emissions resulting from photochemical reactions is negligible during daylight hours compared with the intensity from photoexcitation. Photochemical reactions are significant at night since there are obviously few direct solar photons. Photochemical reactions are not specifically addressed in this analysis because the data was obtained during the daylight period.

Photoexcitation is the excitation of an atom as a result of the absorption of a photon. The atom drops back to a lower energy state by emitting a photon with energy equal to the transition. This process will be further described in the next section on molecular emissions.

B. Molecular Spectra

Molecular emissions may occur as the result of electronic state changes, but they may also occur from purely vibrational and rotational changes of state. Figure II-4 illustrates an electronic transition. Each of these types of transitions has typical energy gaps, with electronic being on the order of 10 eV, vibrational of .1 eV, and rotational of .001 eV.

8

As seen in the figure, for any given electronic energy level there are many vibrational energy levels labeled v' for the excited electronic state or v" for the lower or ground electronic state. Similarly, for a given change in vibrational level there are many possible initial and final rotational levels. As a result, molecular emissions from one vibrational to another are composed of many closely spaced lines. These emissions are called molecular bands.

The principal photon-molecule interactions are shown in Figure II-5. For elastic scattering, an energy transfer between the photon and the molecule does not take place, even though the photon may change direction. With inelastic scattering, the incident photon not only changes direction, but imparts energy to the molecule. In this case, the molecule is excited to a
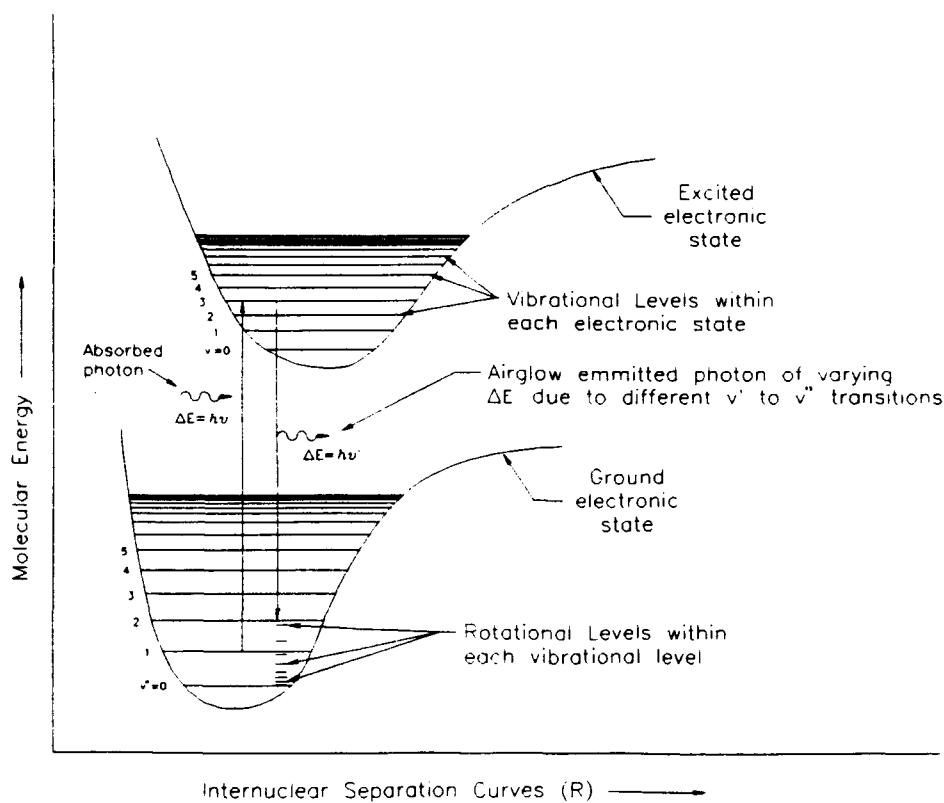
Figure II-4 Molecular energy versus internuclear distance.

9

higher energy state. If the energy difference between states is equal to a level ΔE, then the deflected photon will propagate with an energy ΔE less than the initial photon's incident energy. Another photon with this energy ΔE will be emitted when the molecule returns to the ground state. Resonance scattering is initiated when the incident photon is absorbed, raising the molecule to an excited state. This is followed by a re-emission when a photon with wavelength equal to the incident photon is emitted. Fluorescence scattering occurs when the excited molecule undergoes several downward transitions in returning to the ground state. Each transition generates a separate photon. An excited molecule can also collide with another particle, thus returning to the ground state without emitting a photon. This is called collisional de-excitation or quenching.

Similar to photon-molecule collisions, electron-molecule collisions may be elastic or inelastic. With inelastic collisions, the molecule is excited to a higher energy level and the electron loses kinetic energy. Photon emissions occur when the molecule drops from the excited state to the ground state. The primary interactions considered for this study are photon-molecule inelastic scattering and flourescense scattering.

10

Figure II-5 Molecular processes induced by incident radiation.

III.   DAYGLOW EMISSION FEATURES

A. Molecular Nitrogen

Figure III-1 is an N_2 energy level diagram including the two transitional bands of interest in the 1800-3400 Å range. The states are indicated by molecular notation, and the transitions are identified by name. Since these are forbidden transitions, the excitation is from electron-molecule inelastic scattering.

1. Vegard-Kaplan Bands

The Vegard-Kaplan system is so designated because Vegard discovered the system in 1932, and Kaplan determined the specific wavelengths involved a few years later. The emissions range from 1250 Å to 5325 Å and represent the $A^3\Sigma_u^+ \rightarrow X^1\Sigma_g^+$ transition. In this transition, the total transformation is $+\rightarrow+$, the electronic inversion is $u\rightarrow g$, $\Delta\Sigma = -1$, and $\Delta\Lambda=0$. From the molecule selection rules, this is a forbidden transition, yet it has been observed as an electric dipole emission. A thorough discussion of the band system is given in Meier (1990).

A-state nitrogen molecules are produced by cascading downward from the B and C states or as a result of photoelectron collisions. Because the relationship of emission bands to photoelectron flux is complicated by cascading N_2 molecules and quenching effects, the V-K band is not generally used to infer photoelectron flux.

2. Lyman-Birge-Hopfield

The Lyman-Birge-Hopfield system is the name given to the $A^1\Pi_g \rightarrow X^1\Sigma_g^+$ transition of N_2. The emission bands arising from this transition extend from 1160 Å to 3020 Å and are due to both electric quadrupole and magnetic dipole transitions. Unlike the V-K system, the

upper state of the LBH system can only be populated by direct photoelectron collision excitation. This system can, therefore, be directly used to infer the photoelectron flux. The LBH bands found in the MUSTANG data are observed in the wavelength region from 1800 Å to 2400 Å. An intensive investigation of the LBH emissions observed during the 1990 flight was performed by Mack (1991).

B. Nitric Oxide

Nitric oxide (NO) emissions dominate much of the dayglow data. There are four primary band systems in the range 1800 Å-3400 Å: γ, δ, β, and ε. These NO transitions are generated by photoexcitation. The β bands are several orders of magnitude less intense than the other emissions, so they have been neglected in this analysis. Figure III-2 is an NO energy level diagram including the three transitional bands of interest in the 1800 Å-3400 Å range.

1. Delta Bands

The $C^2\Pi \rightarrow X^2\Pi$ transition band system, designated δ, ranges from 1600 Å to 4300 Å (Barth, 1965). Using standard notation, the upper electronic state's vibrational level is designated v', and the lower state vibrational level, v". The δ transition includes vibrational levels corresponding to v'=0,1,2,3,4 and v"=0,1,...23. Nitric oxide will dissociate at v' > 0 for $C^2\Pi$, so v' is limited to v'= 0 only.

2. Gamma Bands

The γ bands of nitric oxide extend from 1850 Å to 6150 Å. The emissions arise from the $A^2\Sigma^+ \rightarrow X^2\Pi$ transition, and the ground state has v"= 0,...23 as previously stated. The dissociation energy for nitric oxide is lower than the energy of the v'= 4 level in the A state, so only transitions arising from v'= 0,1,2,3 contribute to the synthetic γ spectrum.

3. Epsilon Bands

The nitric oxide ε system is the result of molecules transitioning from $D^2\Sigma^+ \rightarrow X^2\Pi$. The wavelengths of emissions range from 1800 Å to 2400 Å. D-state molecules populate vibrational levels $v'= 0,1,2$.
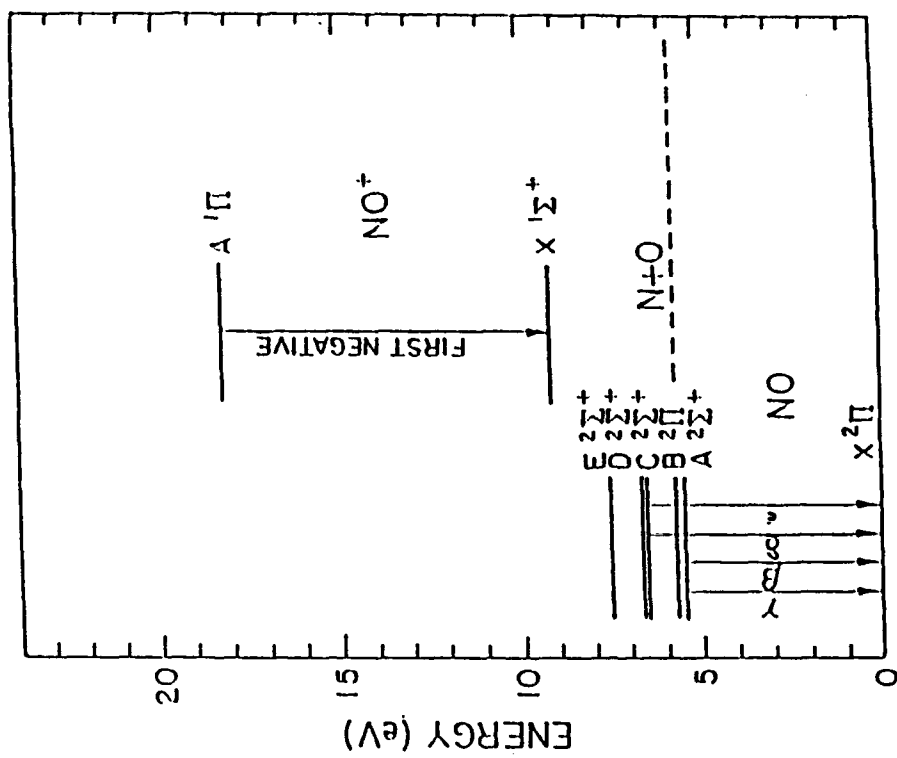
Figure III-2 NO Energy level diagram (Sharp, 1970).
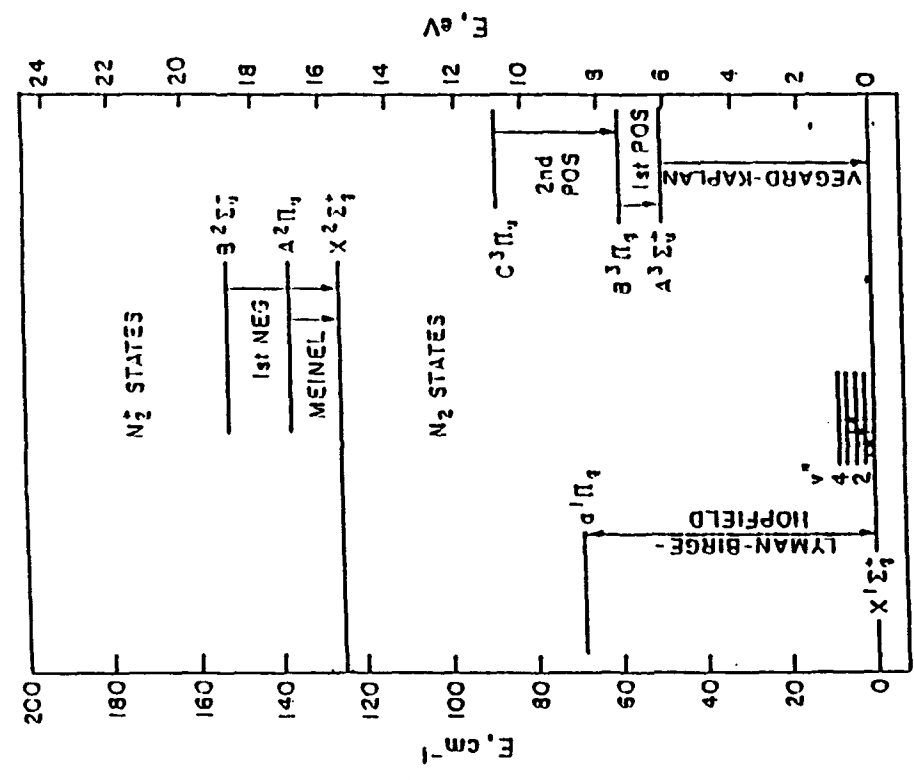
Figure III-1 N₂ Energy level diagram (Sharp, 1970).

15

IV. THE EXPERIMENT

A. Introduction

The middle ultraviolet spectra analyzed in this thesis were obtained from the NPS MUSTANG spectrograph flown on a NASA sounding rocket launched on March 19, 1992, from White Sands Missile Range, New Mexico. The MUSTANG instrument was launched on a Terrier boosted Black Brant vehicle, which carried the payload to an apogee altitude of 320km. The spectrograph field-of-view was pointed in the anti-solar direction with an observation-zenith-angle of 100° on the up-leg and 90° on the down-leg.

B. Instrument Description

The MUSTANG (Middle Ultraviolet Spectrograph) shown in Figure IV-1, covers a wavelength range from 1850Å to 3400Å. It is a modified 1/8 m Ebert-Fastie spectrograph
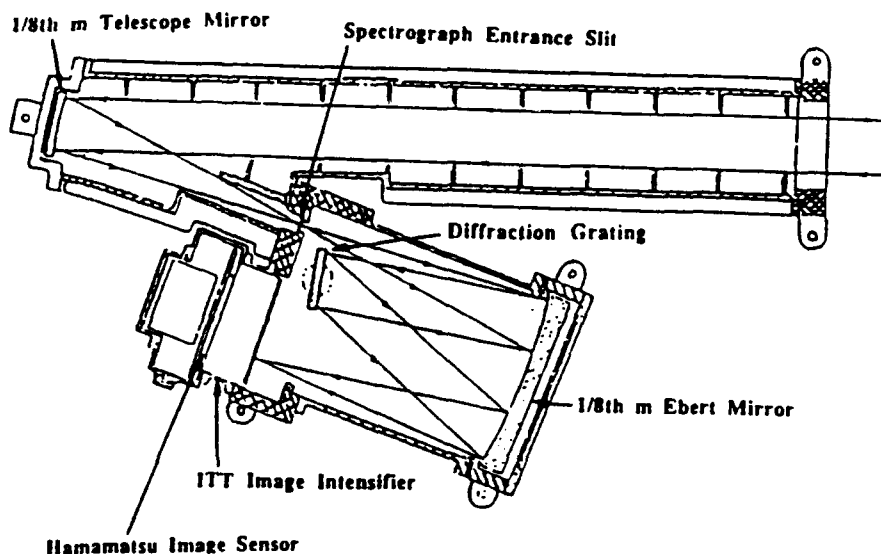
Figure IV-1 Schematic diagram of the MUSTANG instrument.

with a 1/8 m telescope constructed by Research Support Instruments, Inc. The entrance slit is 5 mm by 140 μm which yields a field-of-view of 2.3° by 0.07°. A 10 Å wavelength resolution is provided by a HYPERFINE (Inc.) 1200 lines/mm grating ruling. The detector assembly consists of an ultraviolet-to-visible ITT image intensifier and a Hamamatsu linear array photodiode detector. The image intensifier uses a quartz input window, a CsTe photocathode, and a fiber optic output window. The detector is an array of 512 photodiodes of area 5 mm by 50 μm giving analog voltage outputs proportional to intensity using a fixed 50 msec integration period. This voltage output is fed serially to an A/D converter and then to rocket telemetry via a FIFO shift register.

Pre-launch calibration/sensitivity was obtained using standard techniques with a Deuterium lamp for the wavelength range 1800 Å-2800 Å and a FEL tungsten lamp for the range 2400 Å-3400 Å. The calibration curves obtained from the two lamps agree to within 10%. The MUSTANG instrument experienced no significant degradation in sensitivity (less than 5%) during the launch sequence based on post-flight calibration.

C. Wavelength Calibration

The wavelength calibration was determined using the emission spectra of Mercury and Platinum. The platinum lamp provides 25 spectral emissions in the wavelength region of interest. The design of the MUSTANG instrument is optimized for a bandwidth from 1850 Å to 3400 Å and a dispersion of 3.13 Å/pixel.

The pixel positions on which the selected platinum emissions fell were determined by a rough approximation (± 0.5 Å) of the centroid of each spectral line. The wavelengths of the 25 emissions were plotted versus pixel position. Previous works (Anderson, 1990;

17

Chase, 1992) used a linear best fit calibration procedure. It was decided to attempt a polynomial best fit for this analysis. The polynomial fit was determined to be:

$$\lambda = \left[1848.270 + 3.188N - (1.374 \times 10^{-4})N^2\right] \text{ Å};$$

where N is the pixel number.

D. Data Collection

Over 8000 spectra were collected by the MUSTANG instrument during the rocket experiment. These spectra were averaged into 65 altitude bins, disregarding a few spectra which were contaminated by noise spikes from the instrument's electronics. Each of the 65 averaged spectra covers a 5 km layer that is labeled by its central altitude. The adjusted spectra were then divided by instrument sensitivity. Each spectrum contained 512 intensity values. The first two values were set to zero, because the uncertainty in the instrument sensitivity at the lower wavelength endpoint is extremely large.

V. DATA ANALYSIS

A. Algorithm Techniques

1. Synthetic Spectra

Computer synthetic spectra written by Cleary (1986) were used for the generation of Nitric Oxide δ, ε, and γ and the Nitrogen Lyman-Birge-Hopfield band emissions. The Nitrogen Vegard-Kaplan synthetic model was written by Siskind and Barth (1987). All of the computer code used in this study were written in Interactive Data Language (IDL®), Version 3.1, designed by Research Systems, Inc. The inputs for the synthetic spectrum algorithms were temperature and the calibrated wavelength range of the MUSTANG instrument. The output is an array of 512 intensities corresponding to the instruments wavelength range. Before comparing the synthetic spectra with the data, the synthetic spectra were convolved with MUSTANG's instrument response function. The MUSTANG instrument response was estimated to be an 11-element symmetric slit function (Clayton, 1990; Anderson, 1990; Mack, 1991).

2. Fitting Method

The technique used to fit the synthetic spectra to the data was an iterative process of modifying a linear combination of each band emission system and adjusting separate synthetic and quantum parameters of each emission as necessary. These adjustable parameters are the: 1) Intensity Scale Factor; 2) Molecular Oscillator Strength; and 3) the Franck-Condon Factor.

The intensity scale factor is a relative weight assigned to each band system. It is a best "initial guess" taking into account the combined contributions of other surrounding

19

emissions. For example, the entire N_2 LBH model was assigned a specific scale factor and then summed with all other contributing spectra.

The molecular oscillator strength is a quantum mechanical component for the synthetic models which quantifies the probability of a molecule absorbing a photon in the electronic ground state and transitioning to a specific vibrational level (v') in the excited electronic state. This mechanism of molecular photon absorption is discussed in the background section. For instance, in the N_2 VK synthetic band system, at a temperature of 1125 K, all v'= 3 bands were assigned a scale factor of .7 in order to decrease the intensity by 30% for a best fit.

The Franck-Condon factor is a quantum mechanical element which quantifies the probability of a synthetic emission occurring from a specific vibrational level (v') in the excited electronic state to a specific vibrational level (v") in a lower or ground electronic state. For example, within the NO γ synthetic band system the γ (2,3) emission was observed to be underestimated by 50% but the γ (2,6) was overestimated by 35% and both were assigned a specific scale factor to correct the discrepency.

The adjustable synthetic and quantum parameters designated as the intensity scale factor, molecular oscillator strength, and the Franck-Condon factor will be referred to as the "SQ parameters" for the rest of this work.

B. Intensity Scale Factor Determination

Intensity scale factors were determined by visual inspection for "goodness of fit". An analysis strategy was developed to take advantage of various attributes of NO and N_2 molecular spectra. For example, the N_2 LBH and NO ε band systems are more prominent from 1900 Å to 2200 Å while the N_2 VK and NO γ band systems are more dominant in the

20

2200 Å to 3100 Å range. A time intensive iterative approach was conducted to identify each synthetic band system which had a discrepency with the data. An initial attempt was made to assign one scale factor per band system. However, it was necessary to modify individual emissions. The SQ parameters of these emissions were modified to achieve a best fit synthetic spectrum to the rocket data.

C. Nitric Oxide Self-Absorption

A self absorption model using Holstein transmission functions, developed by Eparvier and Barth (1992), was applied to the NO (0,0), (1,0), (2,0) γ resonance band emissions. The generated synthetic models were then added to other contributing spectra. If the intensities had a discrepency to the data, their respective SQ parameters were modified for a best fit.

D. NO Column Density Determination

The NO column density profile determination was performed in tandem with the temperature profile and NO intensity scale factor estimations. The NO column density (ρ_{col}) for each altitude bin was calculated from the following relationship:

$$\rho_{col} = \kappa * \eta * \zeta \left(\frac{atoms}{cm^2} \right)$$

Where: $\kappa = 3.13 \left(\frac{\text{Å}}{pixel} \right)$ $\qquad$ $\eta = \text{NO intensity scale factor} \left(\frac{R}{\text{Å}} \right)$

$R = 1 \times 10^6 \left(\frac{photons}{cm^2 * sec} \right)$ $\qquad$ $\zeta = \left(\frac{atom * pixel * sec}{photon} \right)$

The κ term is the MUSTANG instrument pixel spacing. The dependence on instrument sensitivity has been removed from the rocket data spectra to yield absolute spectral intensity

21

(η) in units of Rayleighs per Angstrom $\left(\dfrac{R}{\text{Å}}\right)$. A Rayleigh (R) is defined

as $1 \times 10^6 \left(\dfrac{\text{photons}}{\text{cm}^2 * \text{sec}}\right)$. And the ζ term is a conversion factor representing one photon

emitted from each NO atom and detected by an individual pixel of the MUSTANG instrument

per unit time.

E. Temperature Estimations

The temperature of each altitude bin was estimated by isolating an observed molecular

band relatively free of other contaminating spectra. The standard emission used below 160 km

was the NO γ (0,1) at 2365 Å. Above 160 km the N_2 VK system begins to contaminate the

NO γ (0,1). The N_2 VK (0,5) at 2605 Å was used for estimating a temperature profile for all

of the upleg and downleg altitude bins above 160 km.

VI. RESULTS

A. Comparison of Data and Synthetic Spectra

The averaged spectra examined here are for the altitude data bins 110, 160, and 195 km. The primary emission features observed in this MUV spectral region of 1900 Å to 3100 Å include the N_2 Lyman-Birge-Hopfield (LBH), N_2 Vegard-Kaplan (VK), and the NO Gamma (γ), Delta (δ), and Epsilon (ε) bands. All known emissions in this range are used in the fitting routines except OI 2972 Å, OII 2470 Å, OIII 2853 Å, and NII 2143 Å atomic lines.

A comparison of the observed spectra with the synthetic spectrum model in the spectrum for all three of the altitude ranges is shown in Figures A-1 to A-22 in Appendix A. In order to illustrate the basic technique and results of the fitting technique employed for this work, the 160 km data set was used as a sample (Figures A-1 to A-10). The 160 km data set was chosen because the intensities of the NO and N_2 band emission systems were approximately equal.

Figure A-1 illustrates the 160 km NO ε (v'=0) emissions for the range 1900 Å to 2130 Å. The N_2 LBH (v'=3) emissions in the same wavelength range are shown in Figure A-2. Both of these synthetic spectra are given to show the individual contributing emissions of the five band systems. To show a complete band system, the sum of all the N_2 LBH emissions is shown in Figure A-3. Figure A-4 presents the summation of the N_2 LBH and NO ε band systems. Continuing with the step by step additions of the other three band systems, the result is shown in Figure A-5.

The individual emissions were used to identified discrepancies between the data and synthetic spectra. This was accomplished by overplotting several emissions in the wavelength

23

range in question. Once an element was identified as the erroneous contributor (e.g., exceeded or underestimated observed intensities), its respective SQ parameters were modified then resummed for a best fit.

Figure A-5 reveals several interesting features of the 160km data set. Note that only minimum intensity scale factors are applied. One can visually identify the synthetic spectrum exceeding the observed data at approximately 1910 Å, 1980 Å, 2050 Å, and 2095 Å. The synthetic spectrum can also be seen lagging at 2030 Å and 2025 Å.

Figure A-6 presents the data versus wavelength compared with the theoretical, but modified oscillator strengths to v' emissions have also been applied. Notice that the model underestimated the observed intensity at 1910 Å and 1930 Å. To correct this, Figure A-7 shows how modifying the Frank-Condon factors for each erroneous (v', v") emission adjusted the theoretical fit closer to the real data. Figures A-8, A-9, and A-10 repeats this process and displays the entire 160 km data set for 1900 Å to 3100 Å. In addition, all of the altitude data bins at 110, 160, and 195 km are illustrated in Figures A-11 to A-22.

The resulting quantum molecular oscillator strengths (v') and Franck-Condon factors (v") to achieve a best fit for each band emission for all three altitude data sets are listed in Tables 1 through 3 in the Appendix section.

B. Nitric Oxide Bands

The nitric oxide synthetic spectra were substantially contaminated by molecular nitrogen at 160 km. The γ (0,1) is an intensity standard at lower altitudes but is interfered with by surrounding N_2 Vegard Kaplan emissions.

A successful attempt was made to standardize the NO Gamma (γ), Delta (δ), and Epsilon (ϵ) bands by weighing all three systems by the same intensity scale factor. This was

24

accomplished by modifying key values of the SQ parameters for each band emission. The NO Delta (δ), and Epsilon (ϵ) bands were the most difficult to model due to contaminating N_2 Lyman-Birge-Hopfield (LBH) emissions in the 1900 Å to 2120 Å range. The NO Gamma (γ) band system was also contaminated with N_2 VK emissions in the 2200 Å to 3100 Å range, but to a lesser degree.

C. Molecular Nitrogen Bands

At 160 km the Vegard Kaplan bands begin to dominate over all other emissions with the exception of the γ (1,0). Initial analysis indicated two discrepencies of the synthetic spectra concerning these bands. First, a negative 3.13 Å shift (approximately 1 pixel resolution) of the VK synthetic versus data spectra. To correct this discrepency, a modification to the VK synthetic algorithm (VKTERM.PRO) of the initial molecular constants was performed. The TO molecular constant was change from 50203.6 to 50169.0 and the WXEE molecular constant was changed from 14.32 to 11.45. And the second discrepency was the observed relative intensities of the VK (0,5), (0,6), (0,7) bands. The synthetic predicted a constant ratio of these three emissions over all temperature inputs. However, the observed data showed varying scale factors which were matched by modifying the synthetic model and have been recorded in Appendix D, Tables B-1 through B-3.

D. Nitric Oxide Self-Absorption

A self absorption model was made of the theoretical self absorption versus non-self absorption mechanisms of the NO (0,0), (1,0), (2,0) γ resonance band emissions. The Holstein transmission functions applied for this model generated mixed results. The NO (0,0) γ resonance band was consistently overestimated at all three altitudes analyzed. The NO (1,0),

(2,0), γ resonance bands also had to have modifications to their respective SQ parameters, but the results did not indicate any consistency. Figure A-11 through A-14 includes the NO γ resonance bands at 110 km.

E. Nitric Oxide Column Density Profile

The nitric oxide density profile inferred from the data is determined from all of the recorded altitude bins and is shown in Appendix B, Figure B-1 and Table B-1. These estimated densities are consistent with other observations during similar solar cycle intensities.

F. Temperature Profile

A temperature profile estimated from the data is determined from all of the recorded altitude bins and is shown in Appendix C, Figure C-1 and Table C-1. These estimated temperatures are consistent with other observations during similar solar cycle intensities.

VII. CONCLUSIONS

A. Summary of Findings

In this work, spectra from the Earth's ionospheric dayglow obtained from a sounding rocket-launched experiment were analyzed. Computer generated spectra were created for the NO γ, δ, and ε bands and the N_2 LBH and VK bands. These synthetic spectra were fitted to the observed dayglow data. An overall synthetic fit agreed well with the observed spectra. Intensity scaling factors, molecular oscillator strengths and Franck-Condon factors were used and modified to obtain a best fit. Synthetic emission bands that were observed to be in discrepency with the observed data were visually identified and corrected to obtain a best possible fit.

The NO intensity scaling factors were used to infer a NO column density profile. A temperature profile was estimated from the synthetic spectra which best fit the data. The synthetic fit also confirmed the theoretical self absorption versus non-self absorption processes of the NO (0,0), (1,0), (2,0) γ resonance band emissions. NO self absorption is a necessary consideration of any atmospheric nitric oxide analysis scheme.

B. Recommendations For Further Research

The NPS MUSTANG will be part of an operational remote sensing spacecraft. It will be launched on the Advanced Research and Global Observation Satellite (ARGOS) in late 1995. Considering the time intensive nature of a visual analysis by comparing the observed data with synthetic spectra, a high speed central processor is strongly recommended. Once an intensive catalog of synthetic emissions (which are in discrepency with observed airglow) is complete,

27

appropriate modifications to the fitting programs would add to the reliability of MUSTANG as

a surveyor of ionosperic parameters for national defense agencies.

VIII. APPENDIX A

Appendix A contains the figures of rocket data versus wavelength and comparing the data with the generated theoretical spectrums as referred to in the results section.

Figure A-1   Comparison of rocket observations at 160km with total synthetic spectrum and synthetic NO ε spectrum for v'=0.
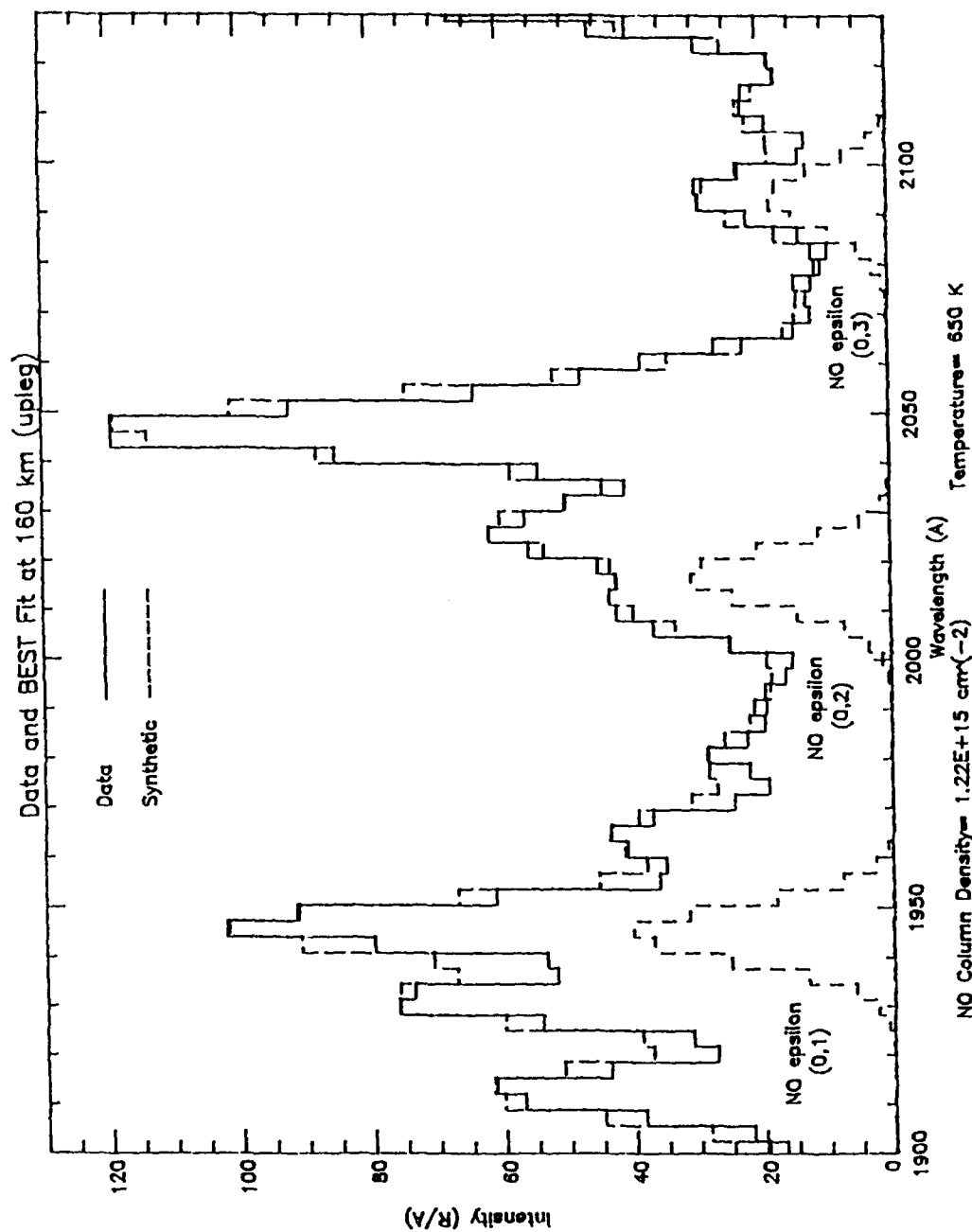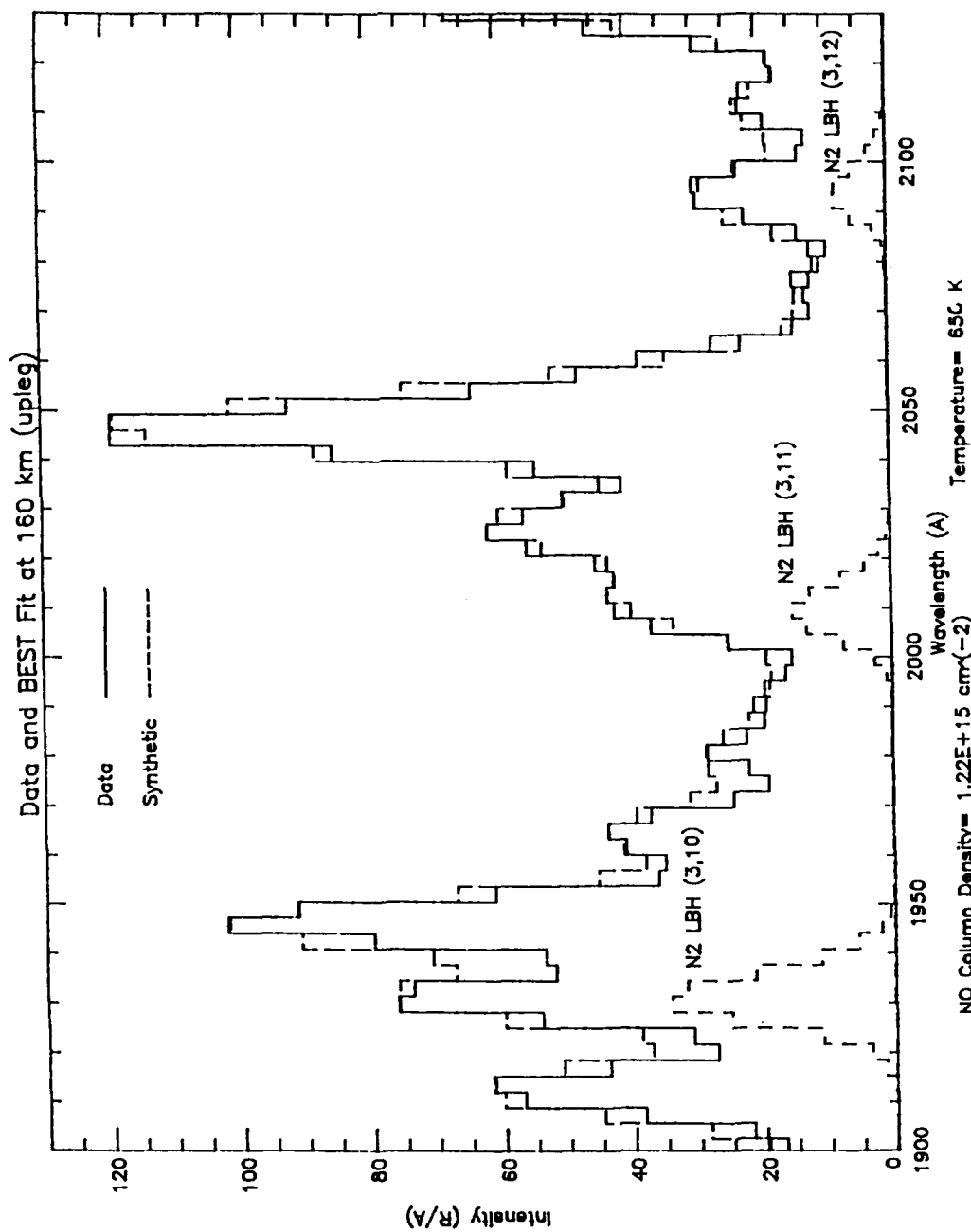
Figure A-2   Comparison of rocket observations at 160km with total synthetic spectrum and synthetic N₂ LBH spectrum for v'=3.

31
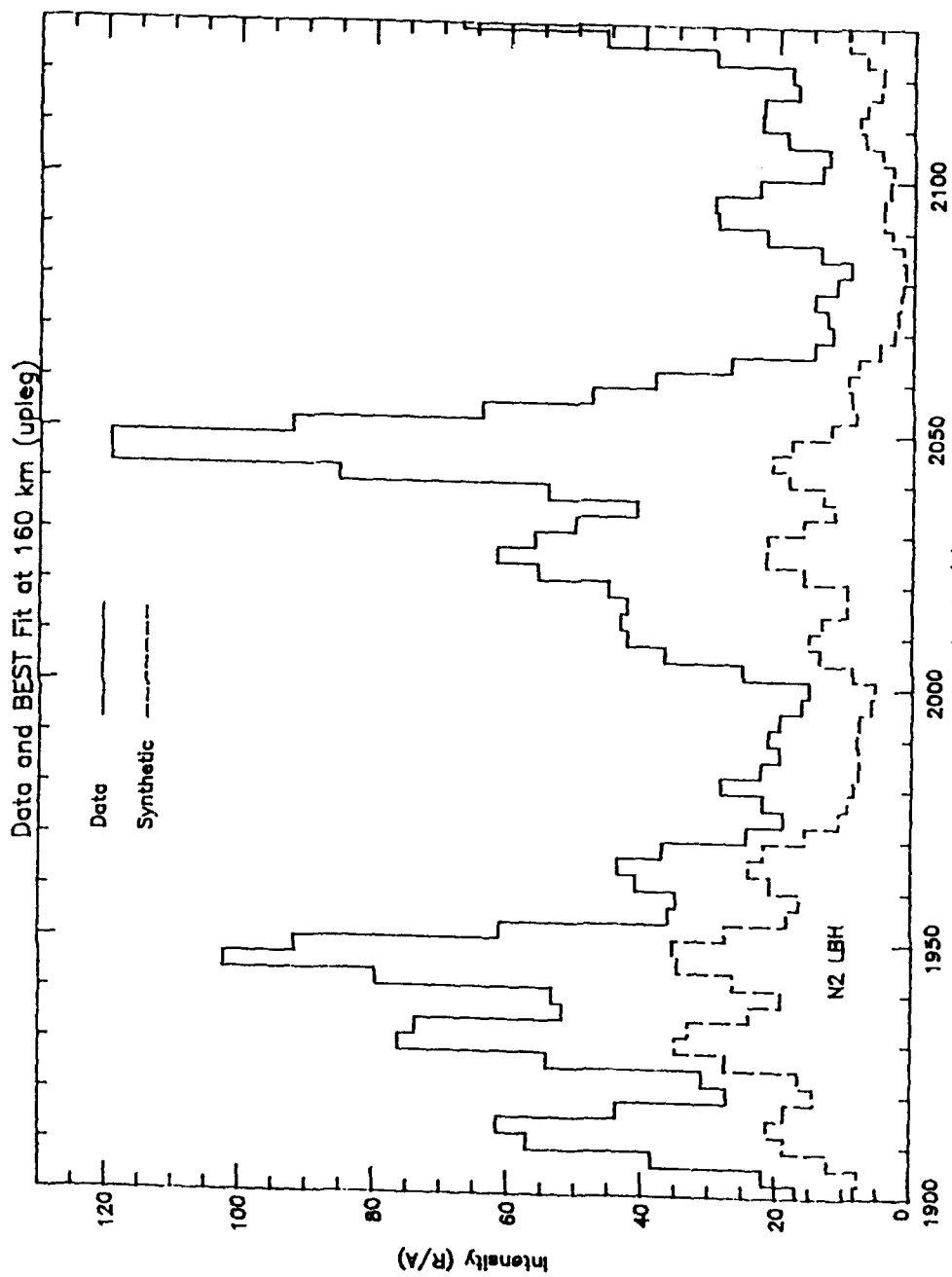
Figure A-3   Comparison of rocket observations at 160km with total synthetic N_2 LBH spectrum.

32
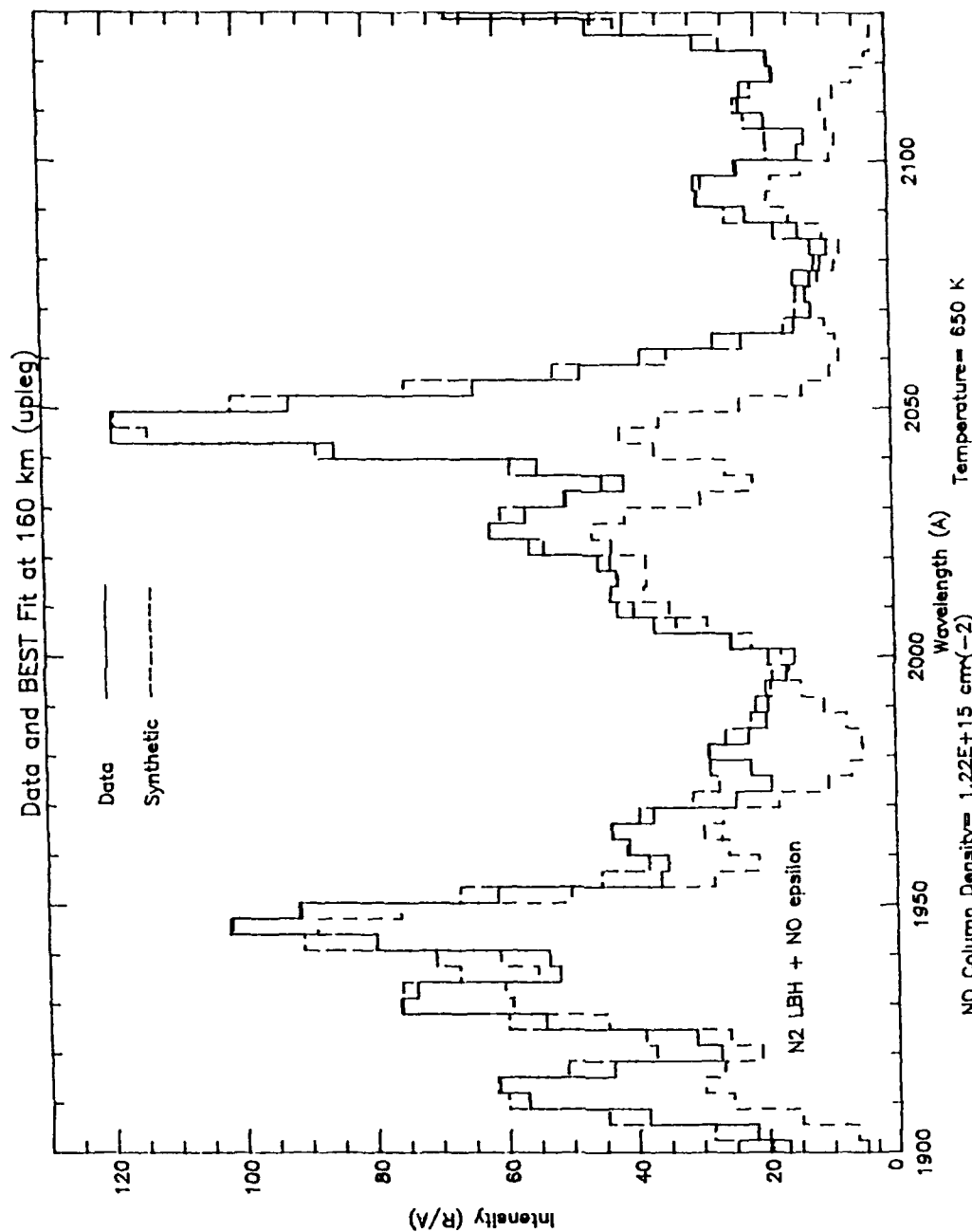
Figure A-4   Comparison of rocket observations at 160km with total synthetic spectrum and total synthetic N_2 LBH and NO ε spectrums.

33

Figure A-5   Comparison of rocket observations at 160km with total synthetic spectrum with only minimum scale factors applied.

34

Figure A-6   Comparison of rocket observations at 160km with total synthetic spectrum with minimum scale factors and modified oscillator strengths applied.

Figure A-7 Comparison of rocket observations at 160km with total synthetic spectrum with minimum scale factors, modified oscillator strengths, and modified Franck-Condon factors applied (Best Fit).

36

Data and Synthetic Fit at 160 km (upleg)

Data ————
Synthetic — — — —

(only minimum scale
factors applied)

NO Column Density= 1.22E+15 cm(−2)   Temperature= 650 K

Figure A-8   Comparison of rocket observations at 160km with total synthetic spectrum with only minimum scale factors applied.

37
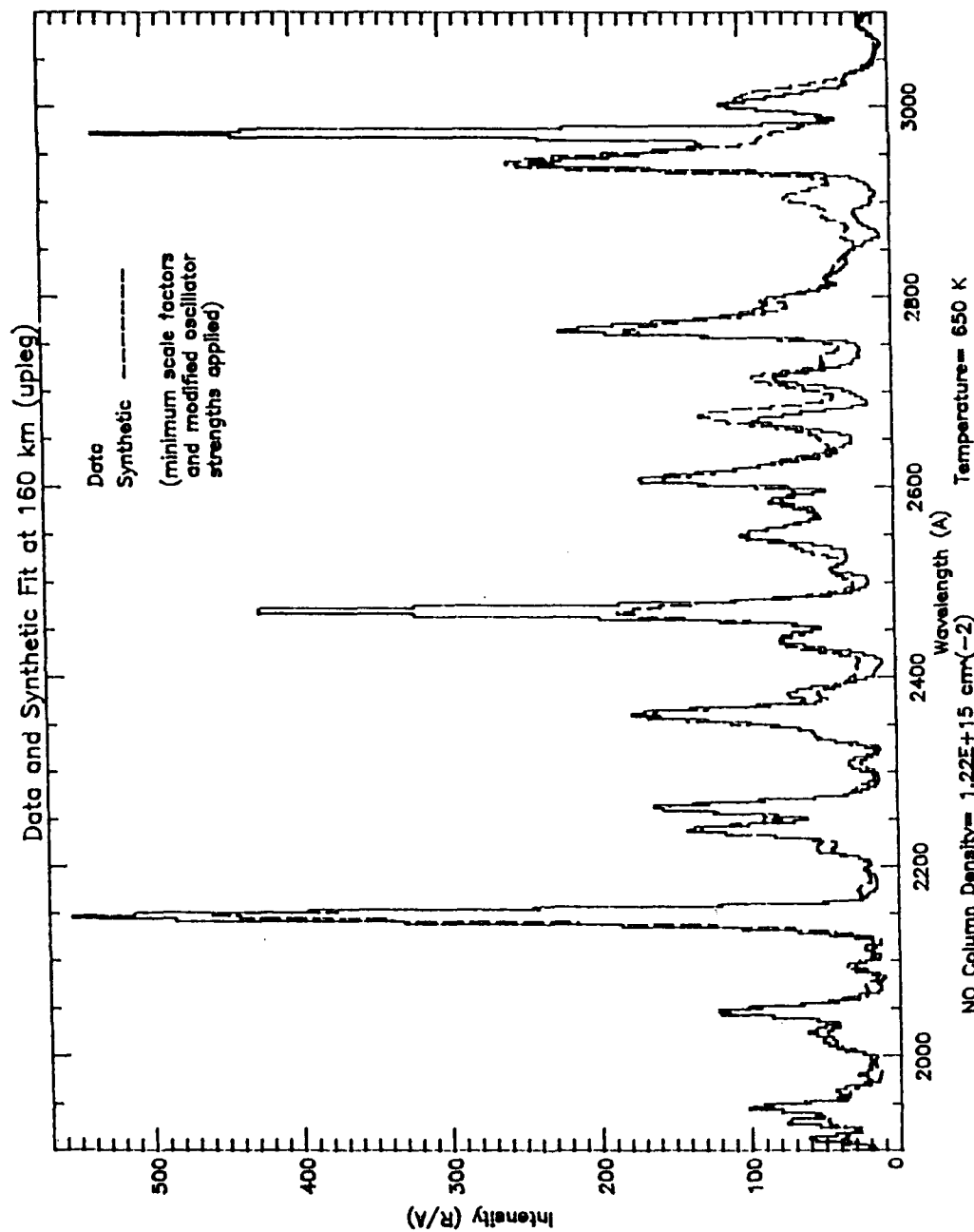
Figure A-9   Comparison of rocket observations at 160km with total synthetic spectrum with minimum scale factors and modified oscillator strengths applied.
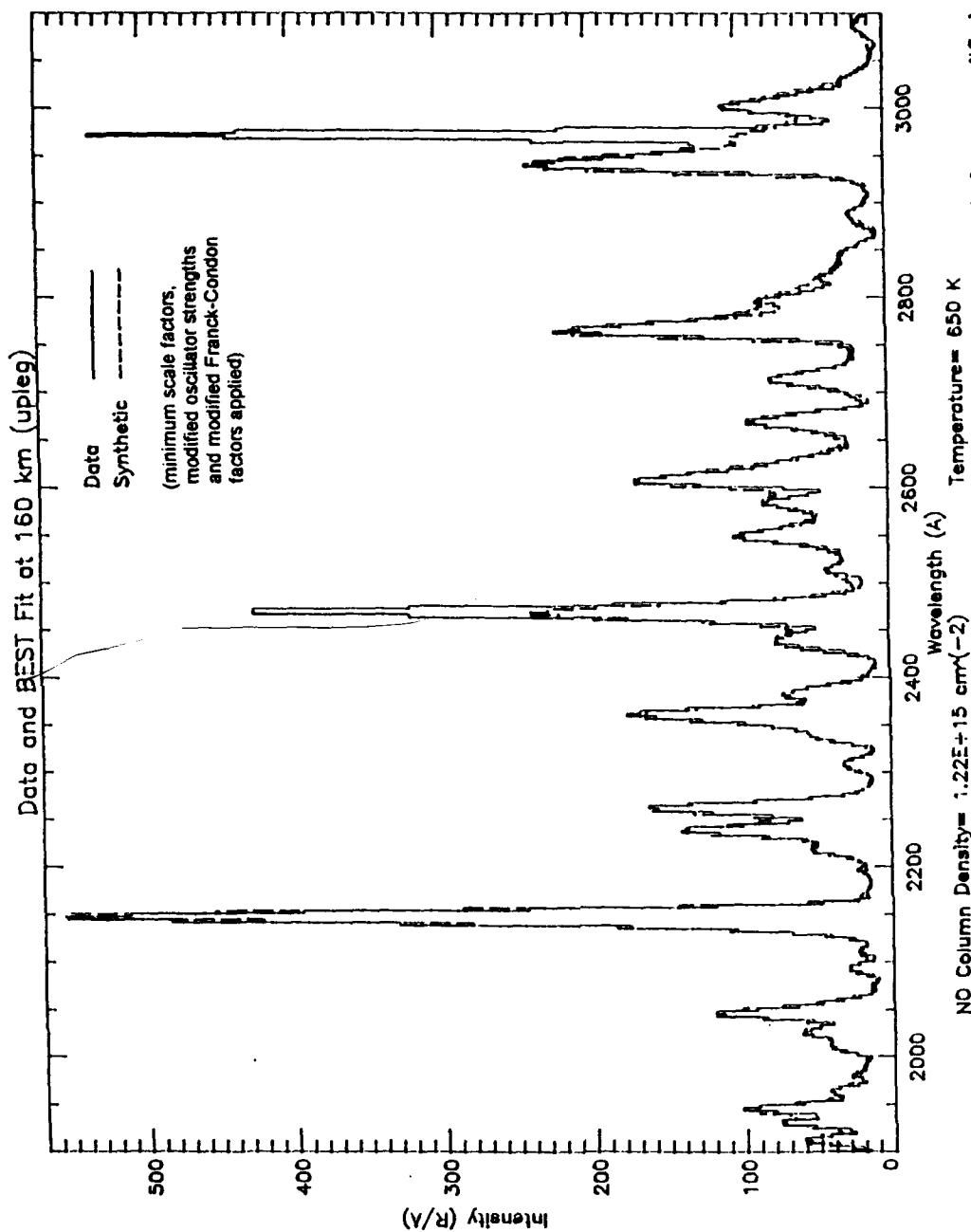
Figure A-10   Comparison of rocket observations at 160km with total synthetic spectrum with minimum scale factors, modified oscillator strengths, and modified Franck-Condon factors applied (Best Fit).
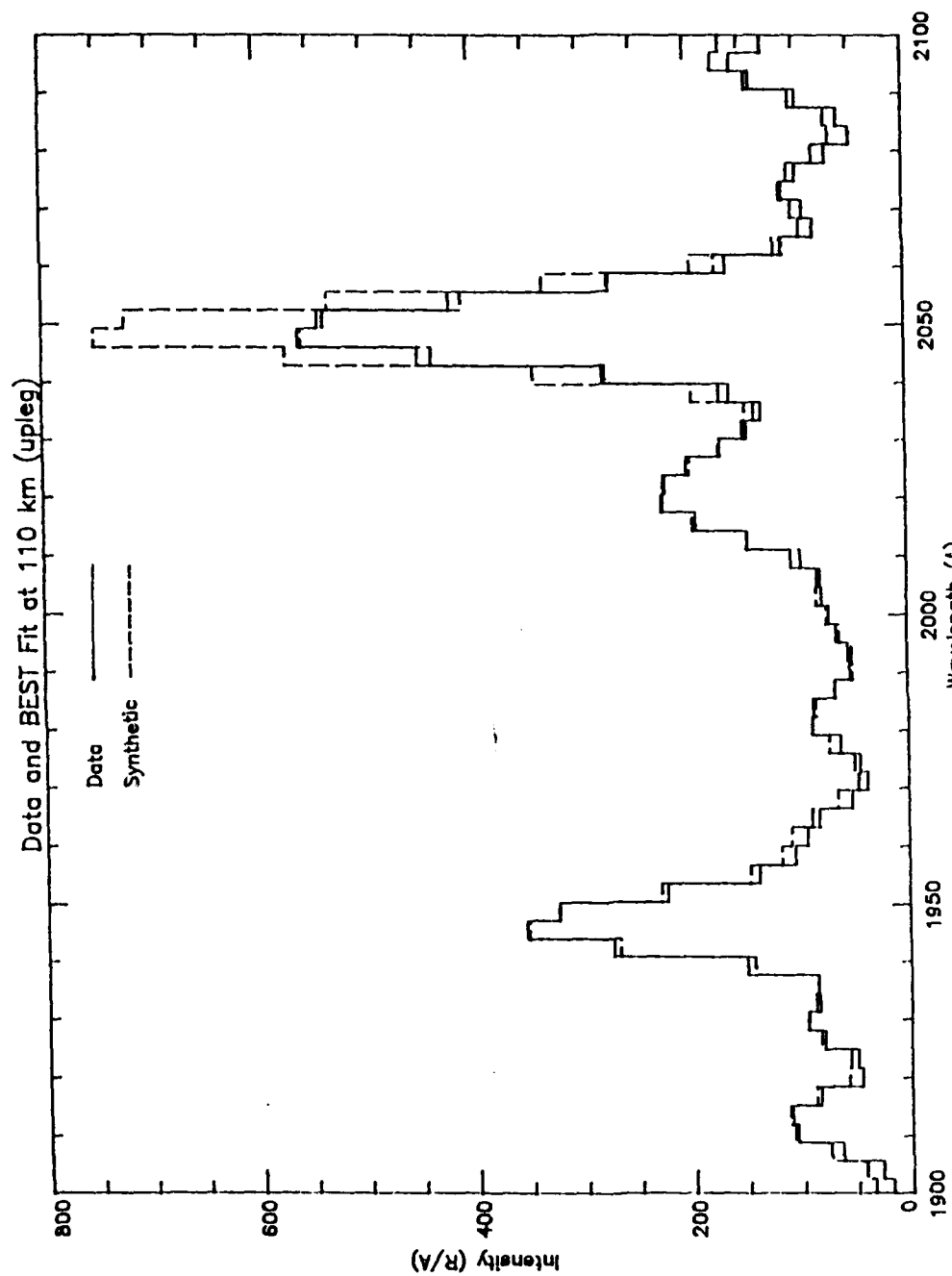
Figure A-11   Comparison of rocket observations at 110km with total synthetic spectrum. One spectrum includes the effects of self absorption and the other does not. Both synthetic spectra include minimum scale factors, modified oscillator strengths, and modified Franck-Condon factors applied (Best Fit).

40
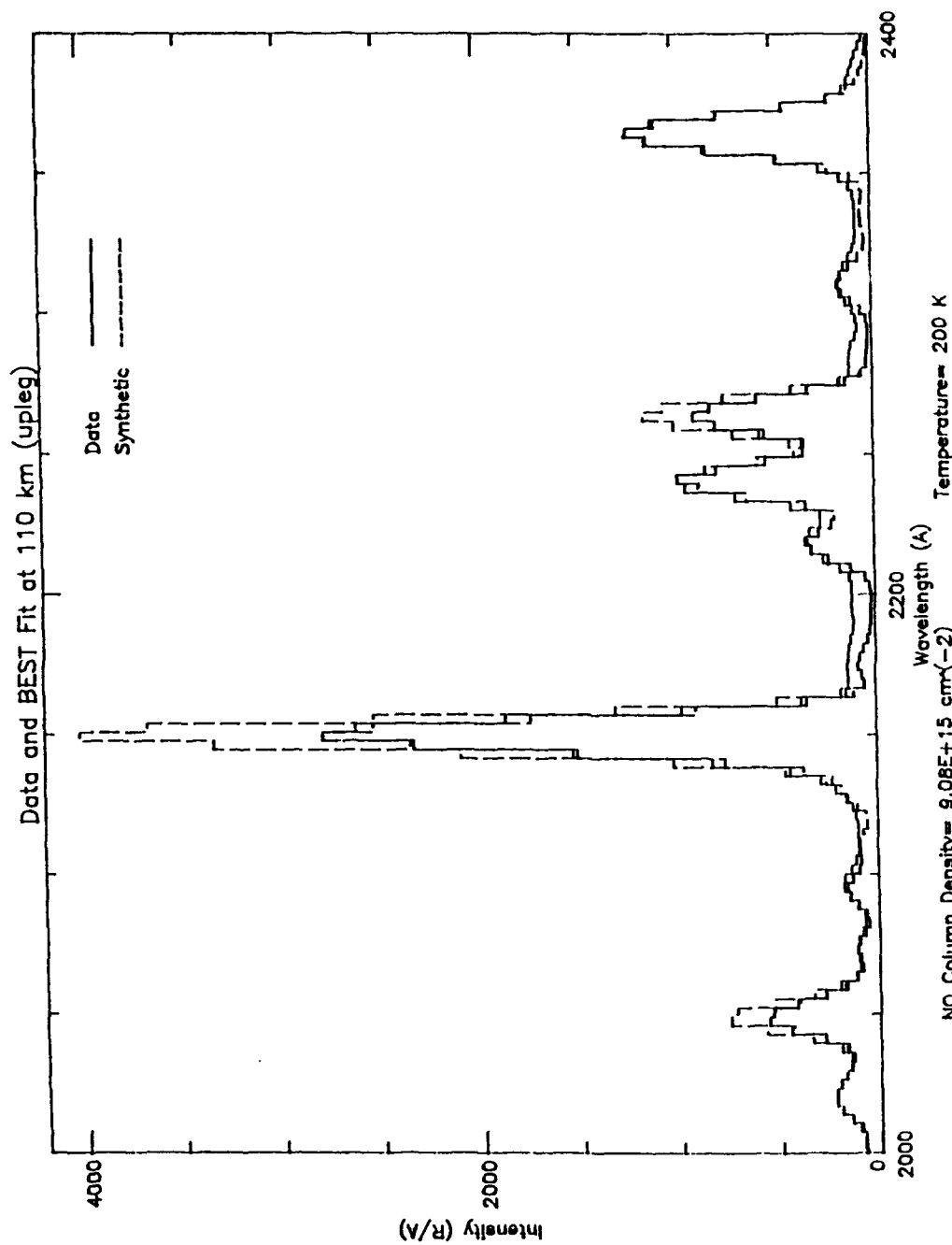
Figure A-12   Comparison of rocket observations at 110km with total synthetic spectrum. One spectrum includes the effects of self absorption and the other does not. Both synthetic spectra include minimum scale factors, modified oscillator strengths, and modified Franck-Condon factors applied (Best Fit).
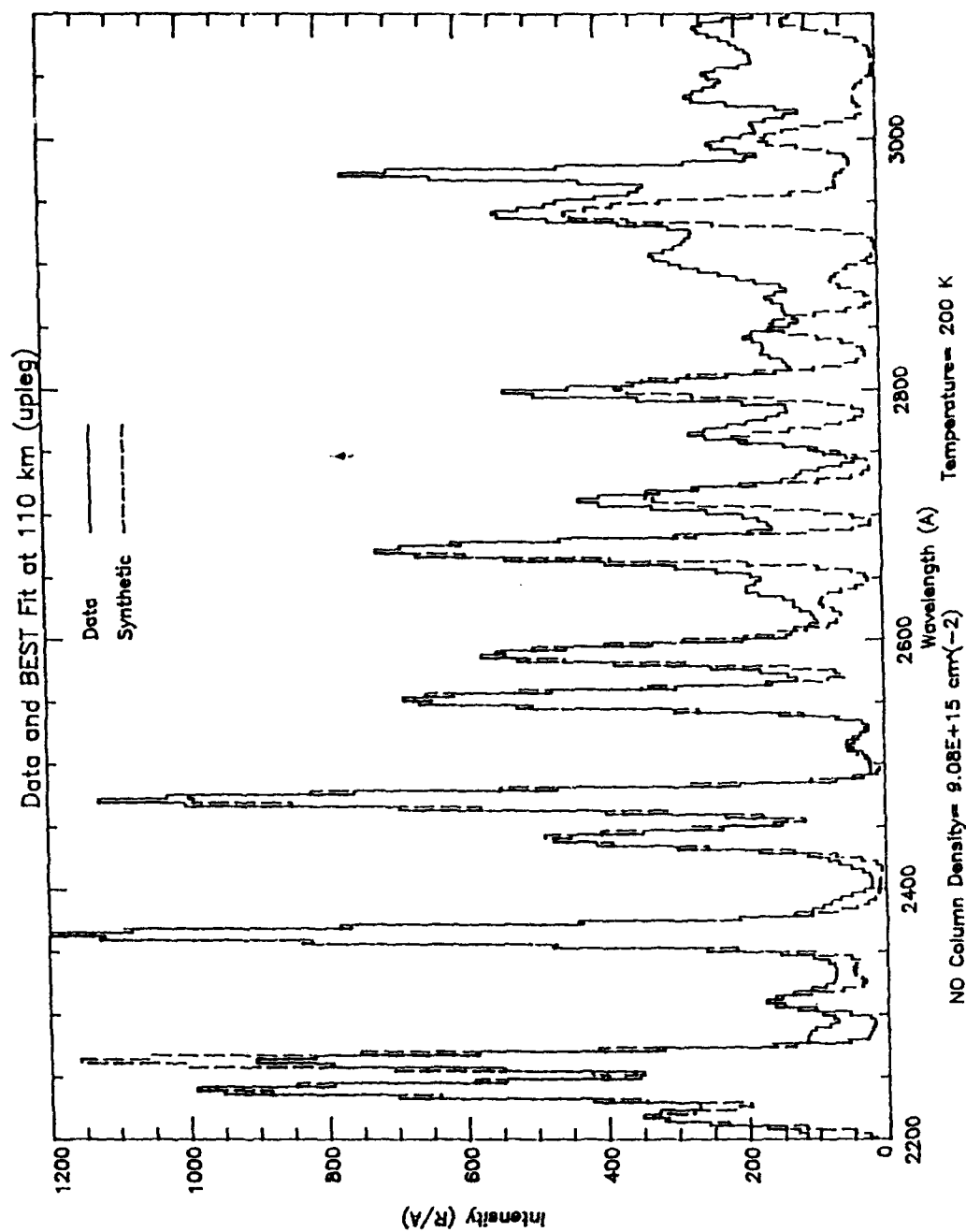
Figure A-13   Comparison of rocket observations at 110km with total synthetic spectrum. One spectrum includes the effects of self absorption and the other does not. Both synthetic spectra include minimum scale factors, modified oscillator strengths, and modified Franck-Condon factors applied (Best Fit).

Data and BEST Fit at 110 km (upleg)
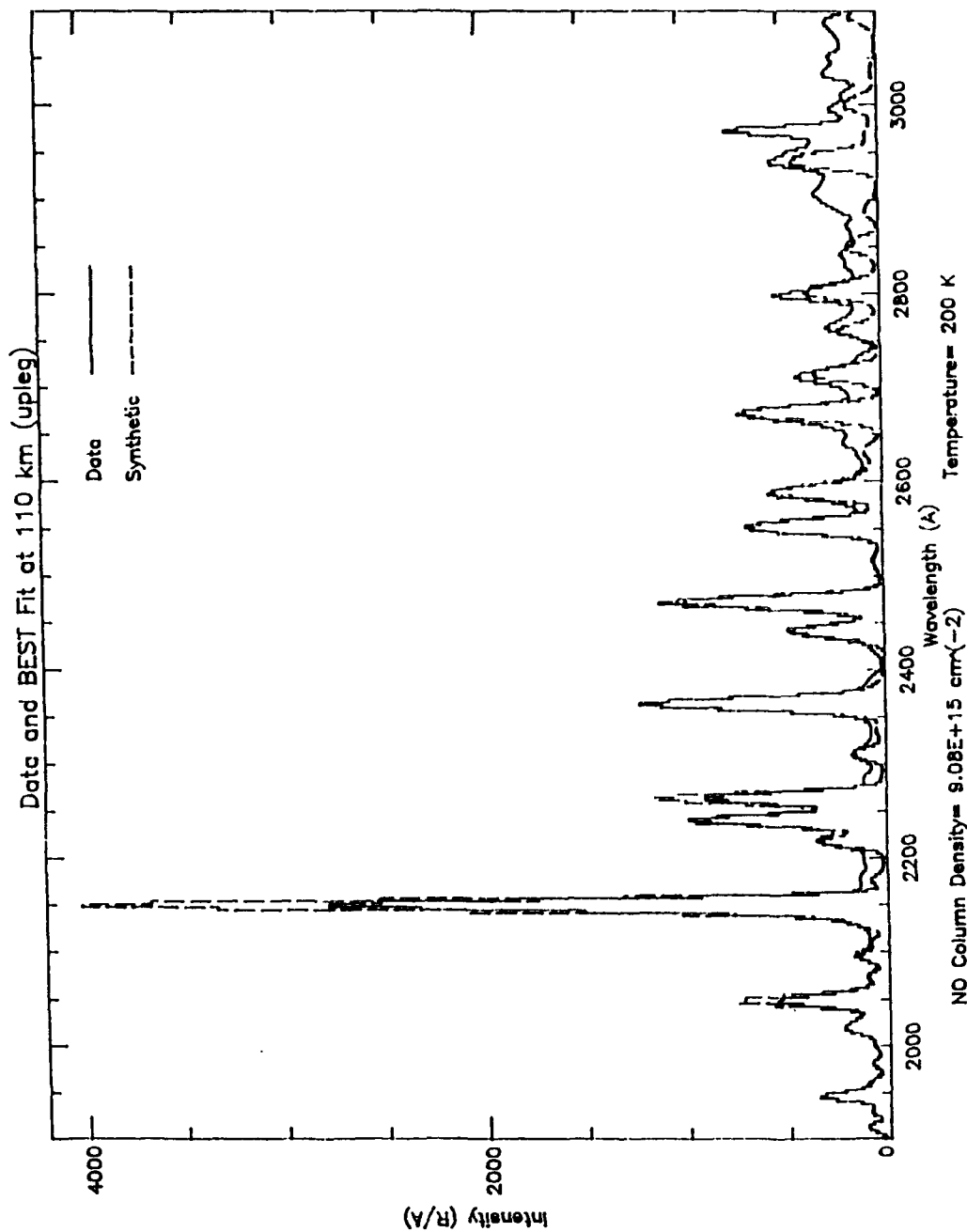
Figure A-14   Comparison of rocket observations at 110km with total synthetic spectrum. One spectrum includes the effects of self absorption and the other does not. Both synthetic spectra include minimum scale factors, modified oscillator strengths, and modified Franck-Condon factors applied (Best Fit).

43
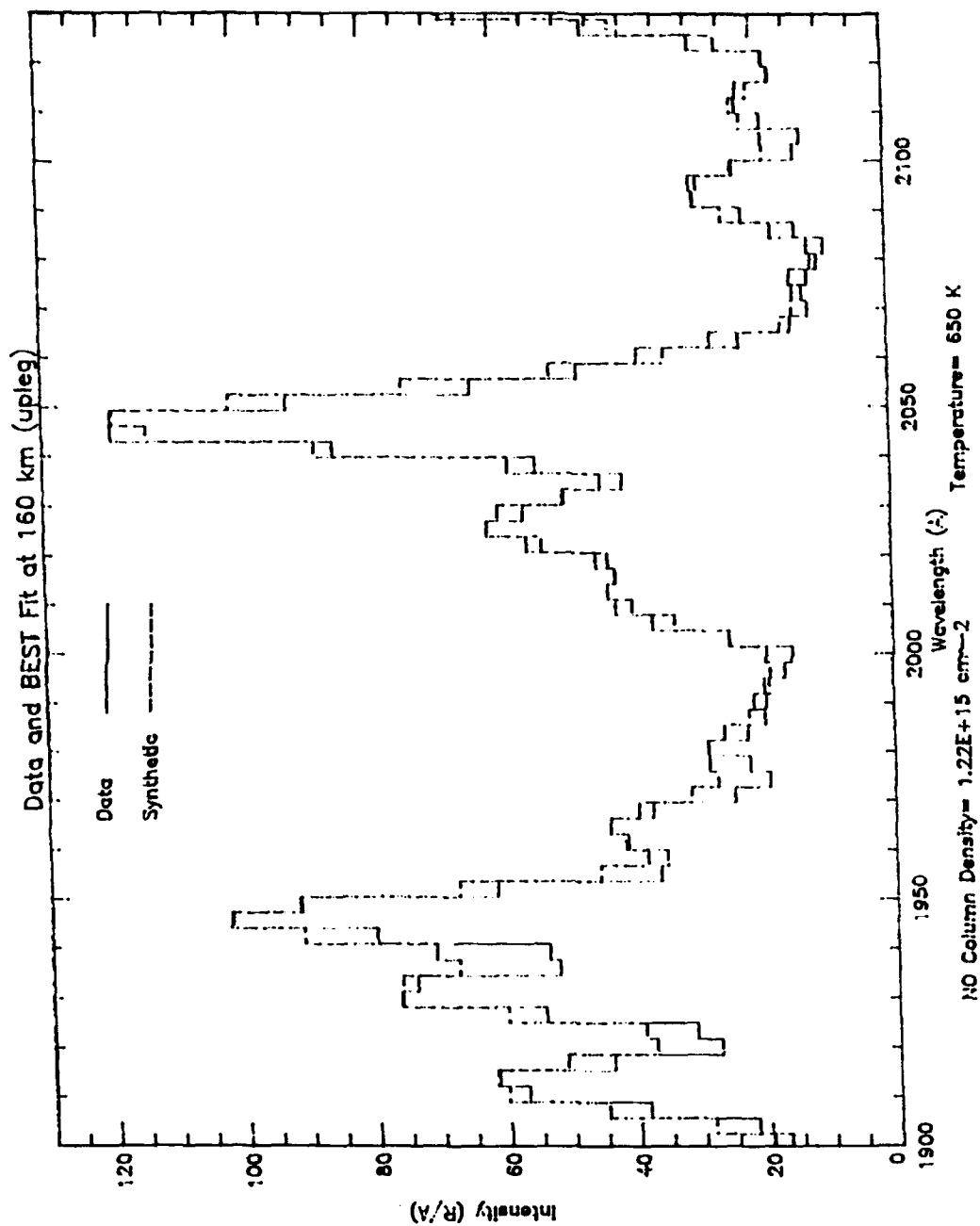
Figure A-15   Comparison of rocket observations at 160 km with total synthetic spectrum with minimum scale factors, modified oscillator strengths, and modified Franck-Condon factors applied (Best Fit).
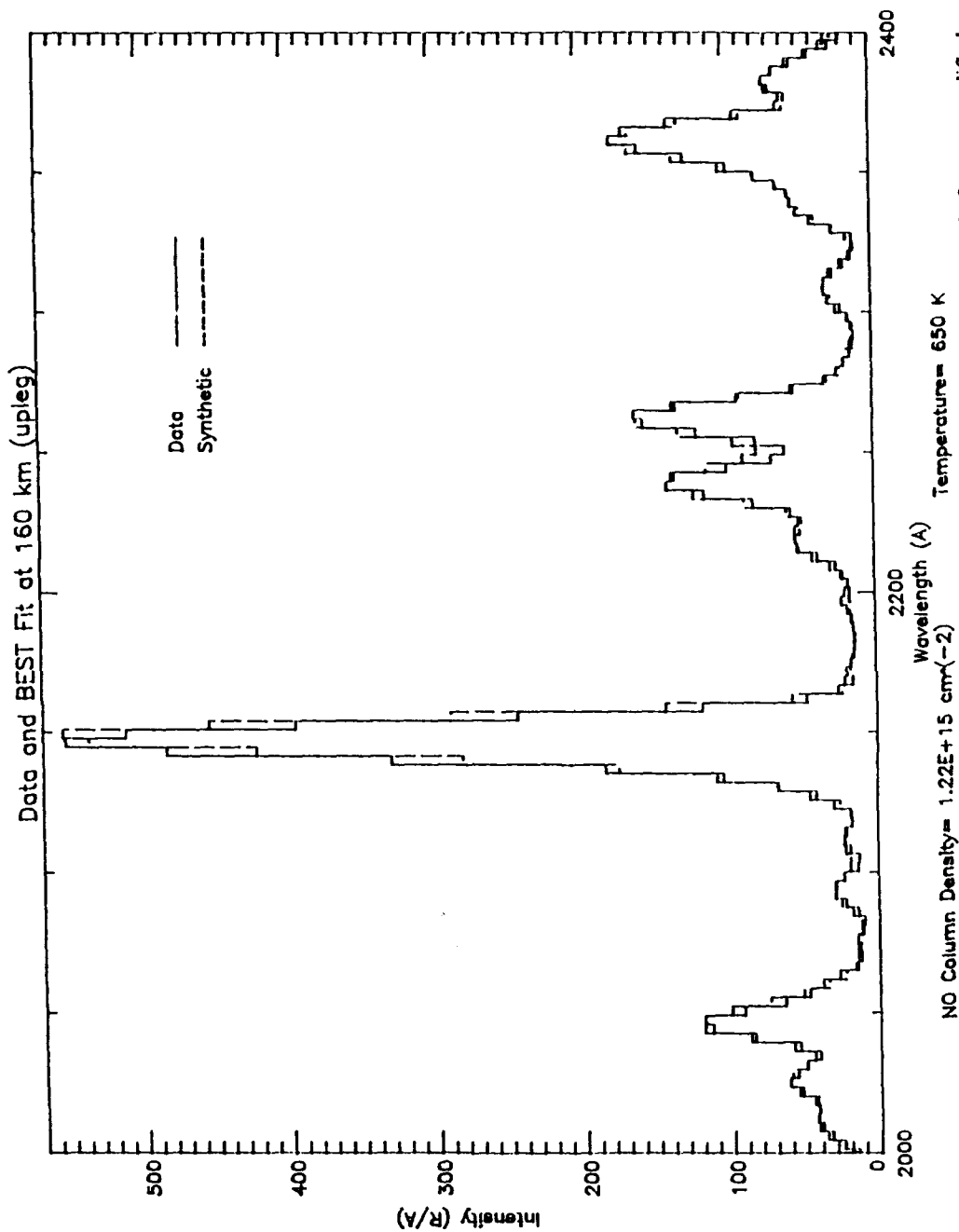
Figure A-16   Comparison of rocket observations at 160km with total synthetic spectrum with minimum scale factors, modified oscillator strengths, and modified Franck-Condon factors applied (Best Fit).

45
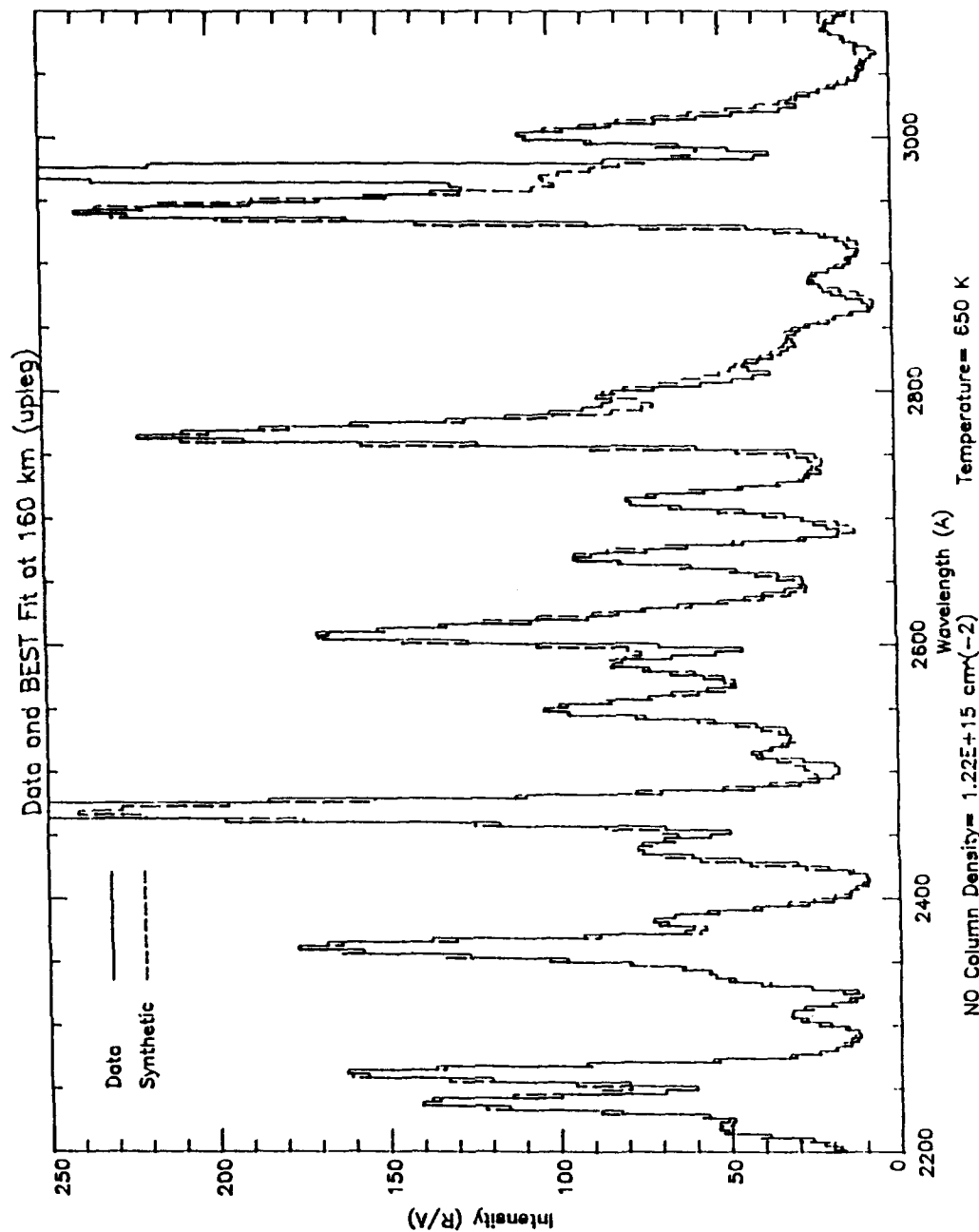
Figure A-17   Comparison of rocket observations at 160km with total synthetic spectrum with minimum scale factors, modified oscillator strengths, and modified Franck-Condon factors applied (Best Fit).
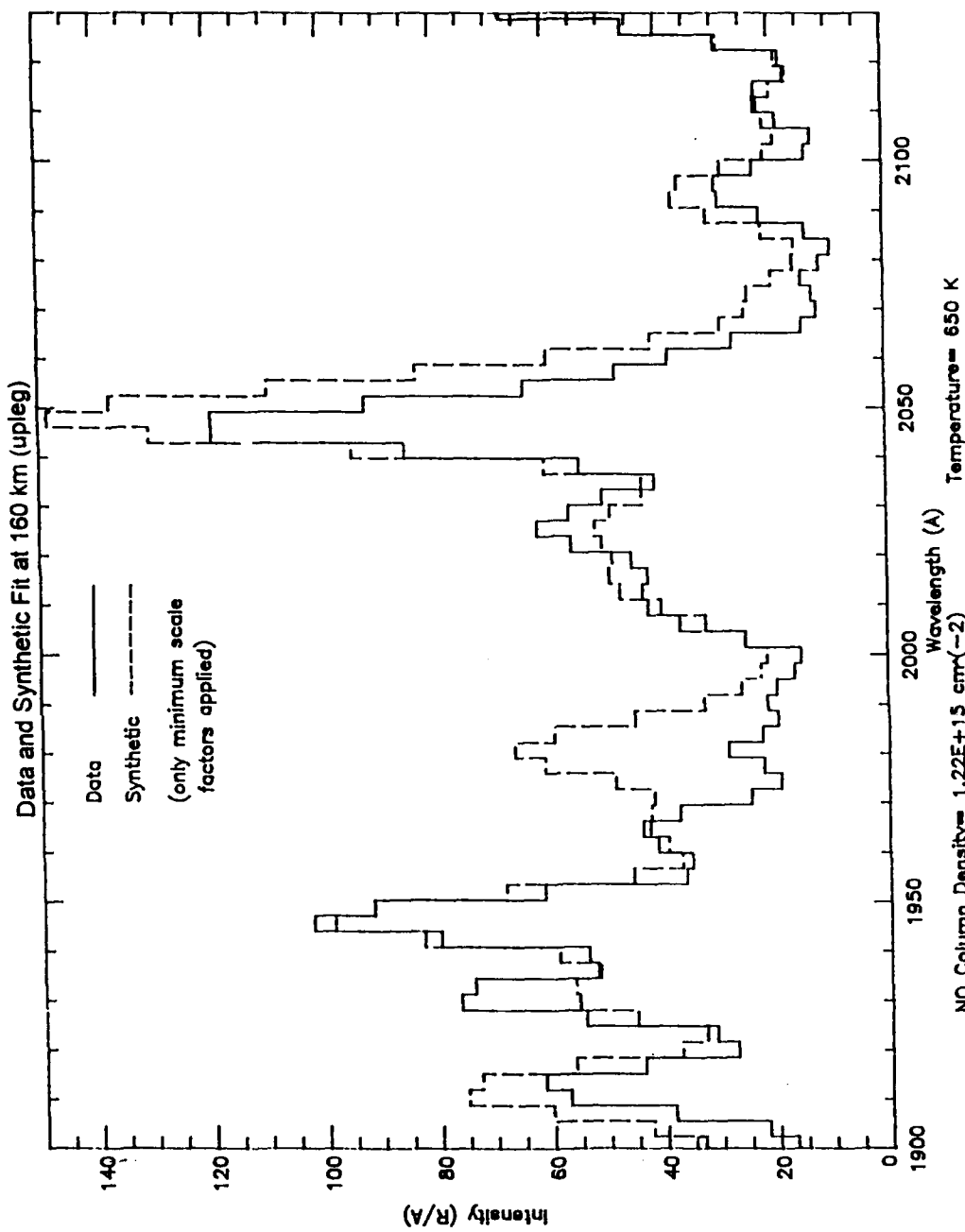
46

Data and BEST Fit at 160 km (upleg)
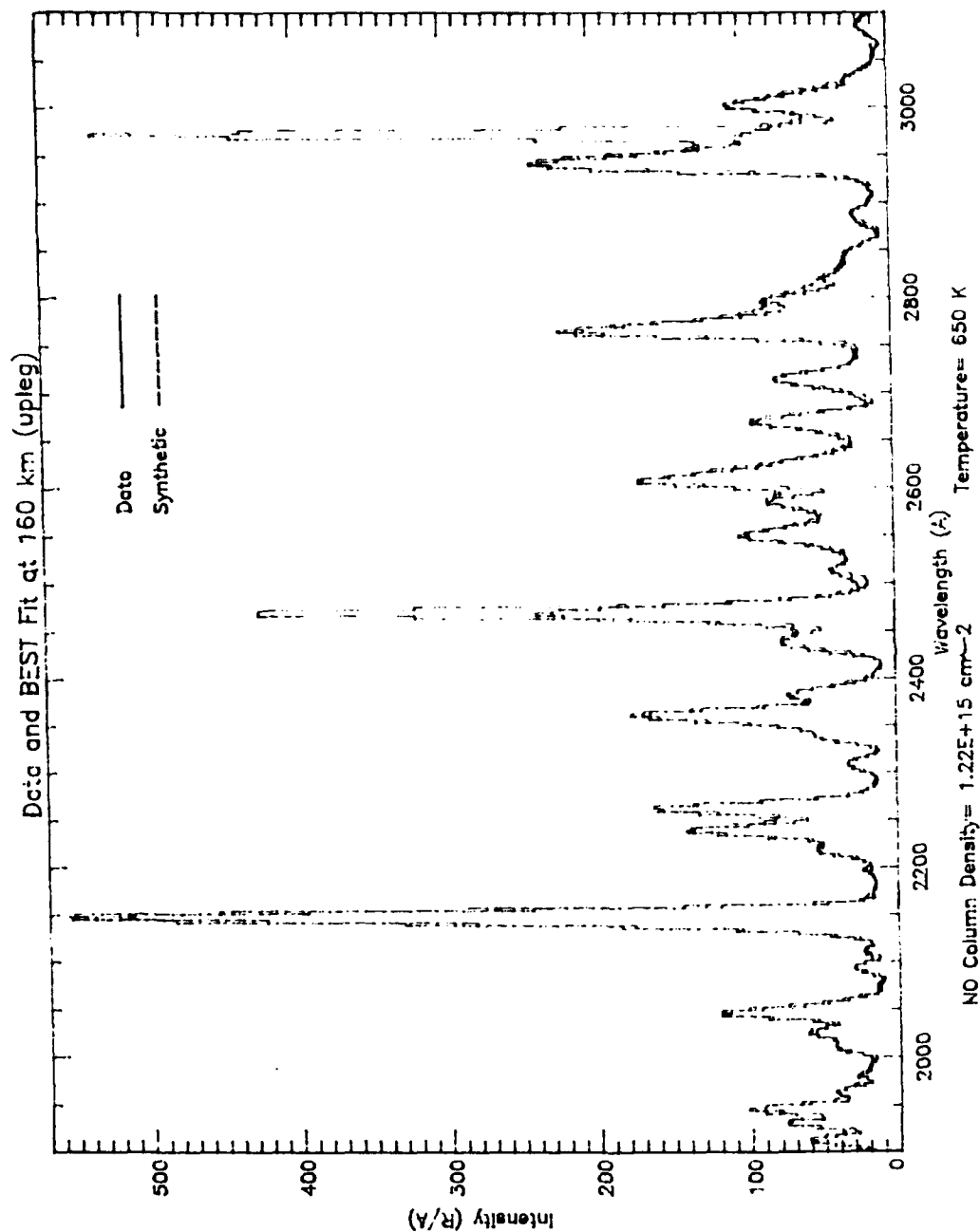
Figure A-18   Comparison of rocket observations at 160km with total synthetic spectrum with minimum scale factors, modified oscillator strengths, and modified Franck-Condon factors applied (Best Fit).

NO Column Density= 1.22E+15 cm−2   Temperature= 650 K

47
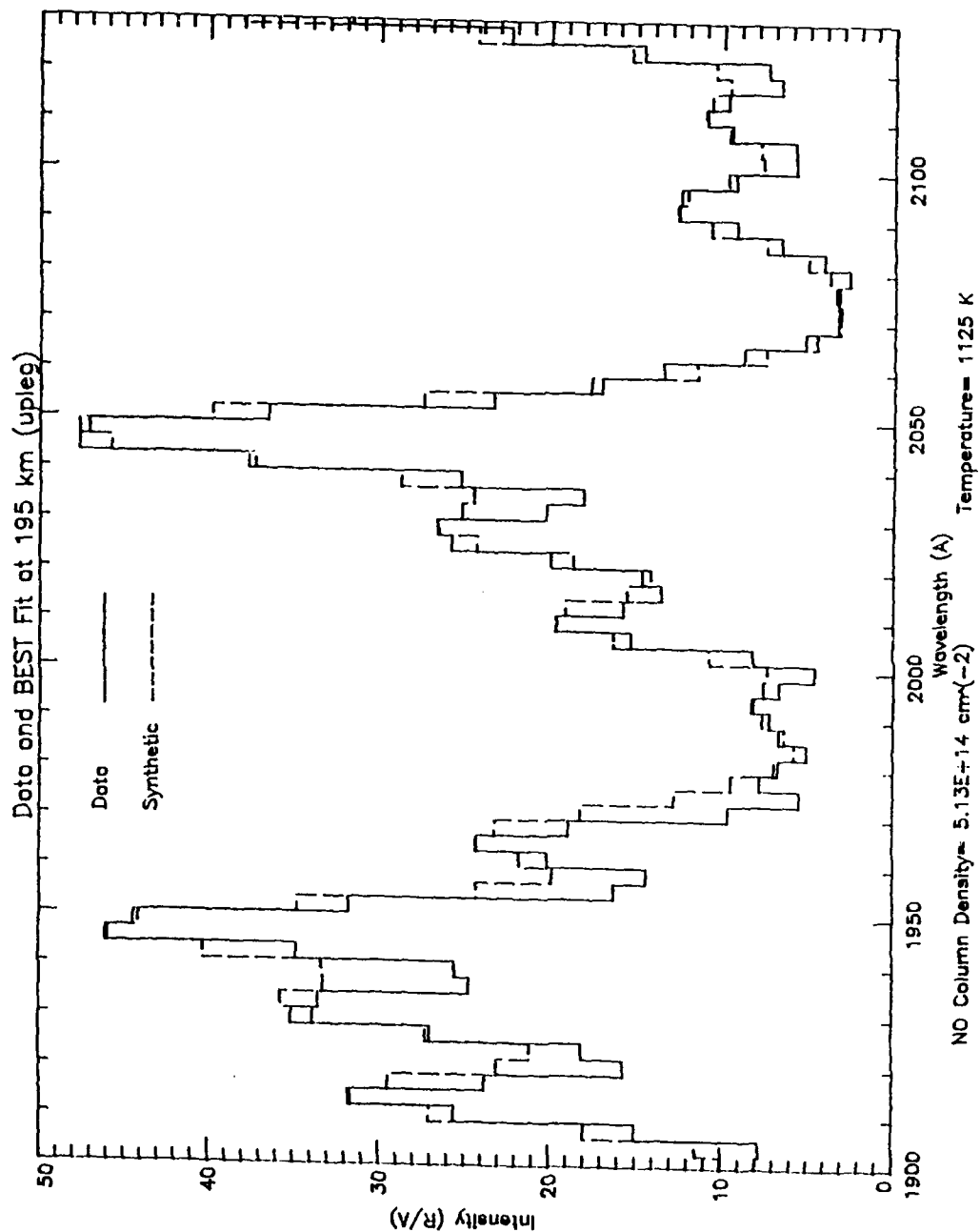
Figure A-19   Comparison of rocket observations at 195 km with total synthetic spectrum with minimum scale factors, modified oscillator strengths, and modified Franck-Condon factors applied (Best Fit).
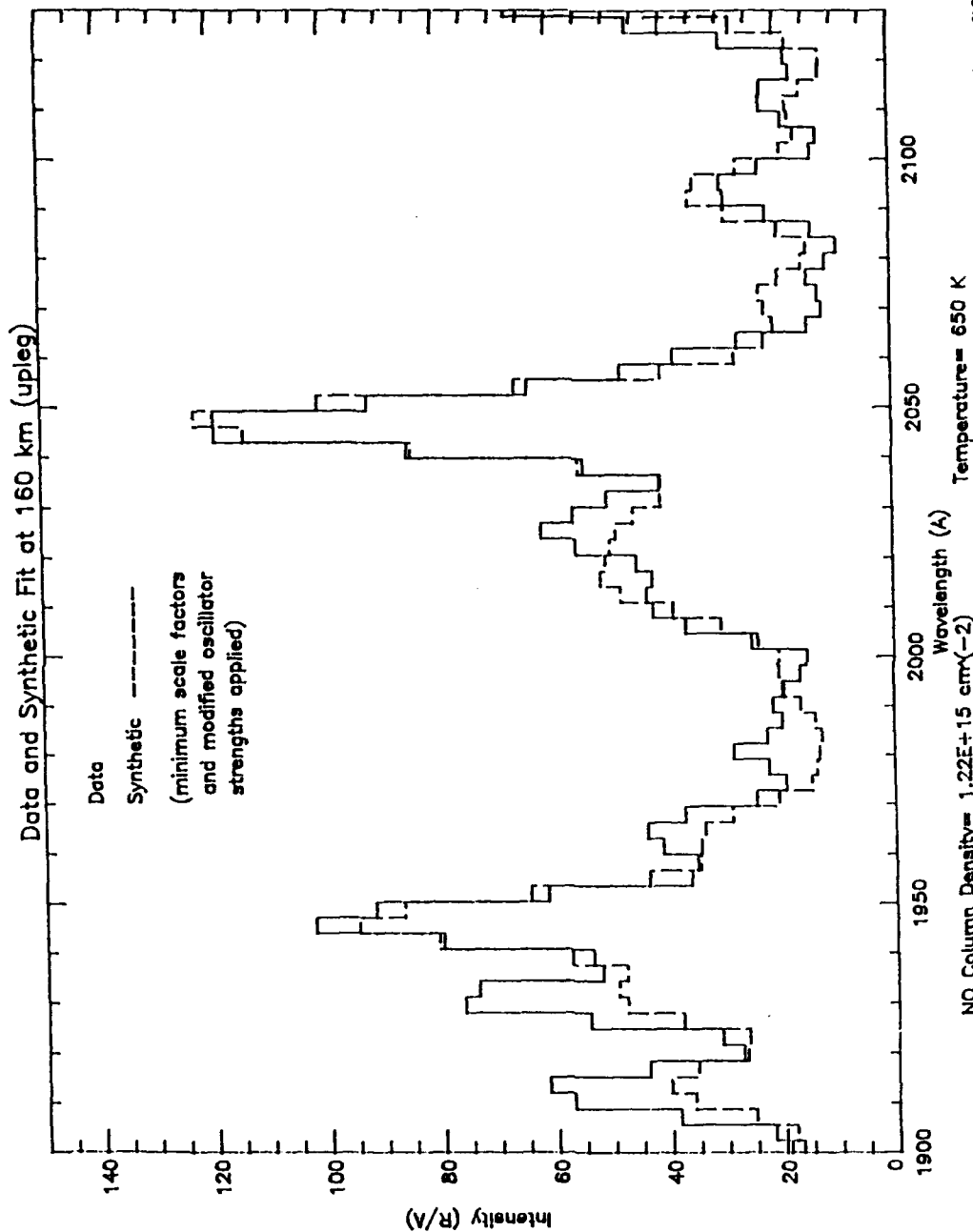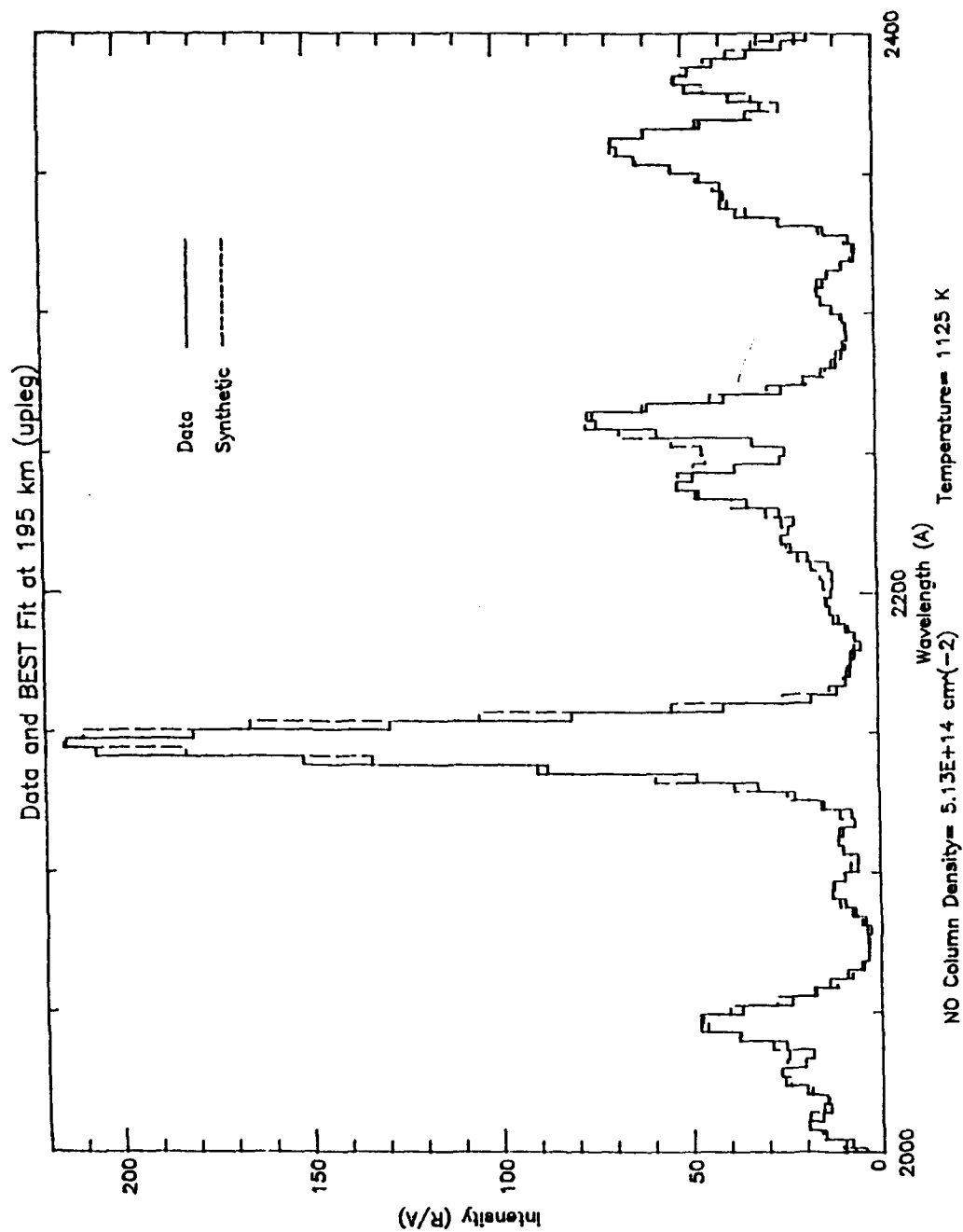
Figure A-20   Comparison of rocket observations at 195km with total synthetic spectrum with minimum scale factors, modified oscillator strengths, and modified Franck-Condon factors applied (Best Fit).
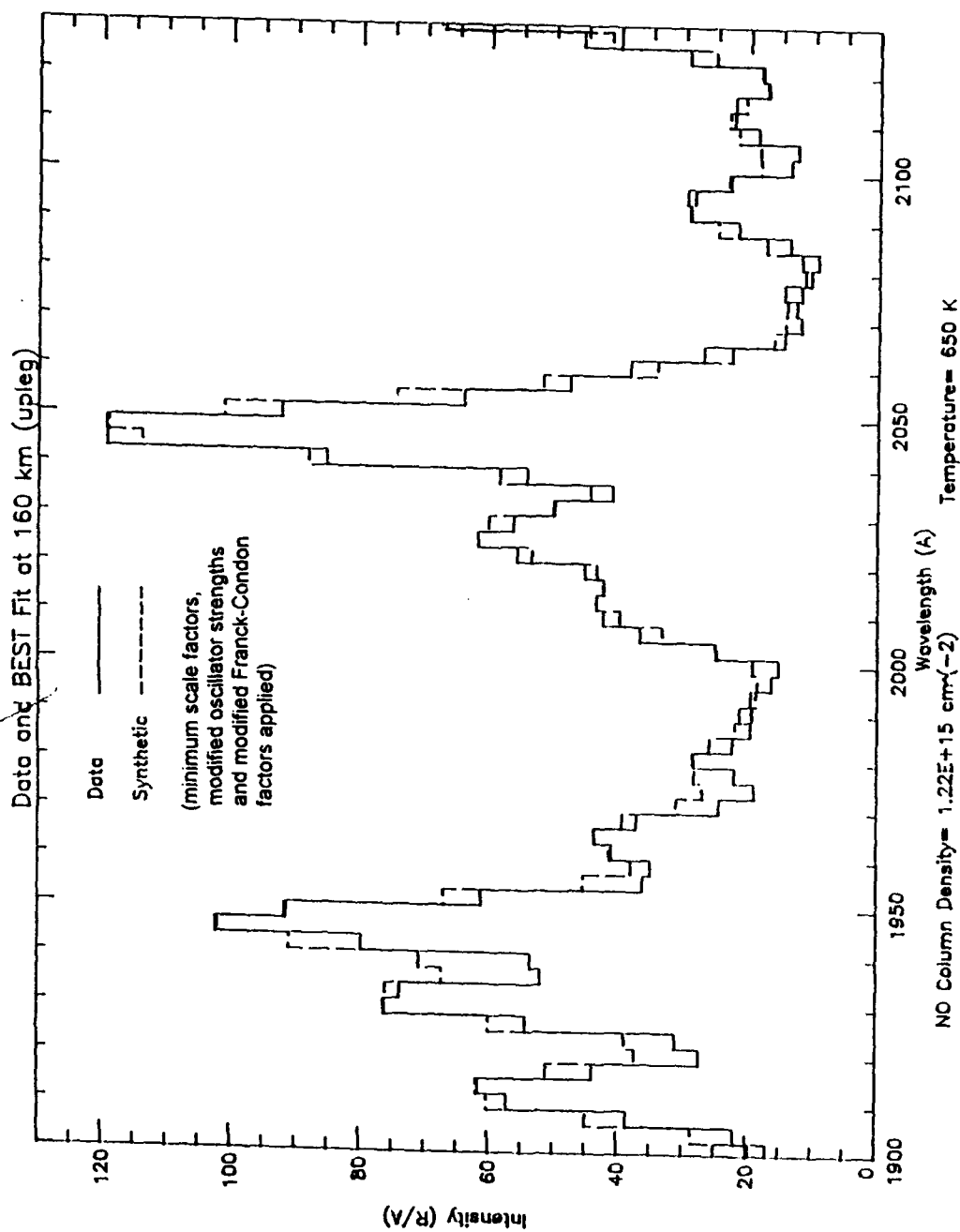
49
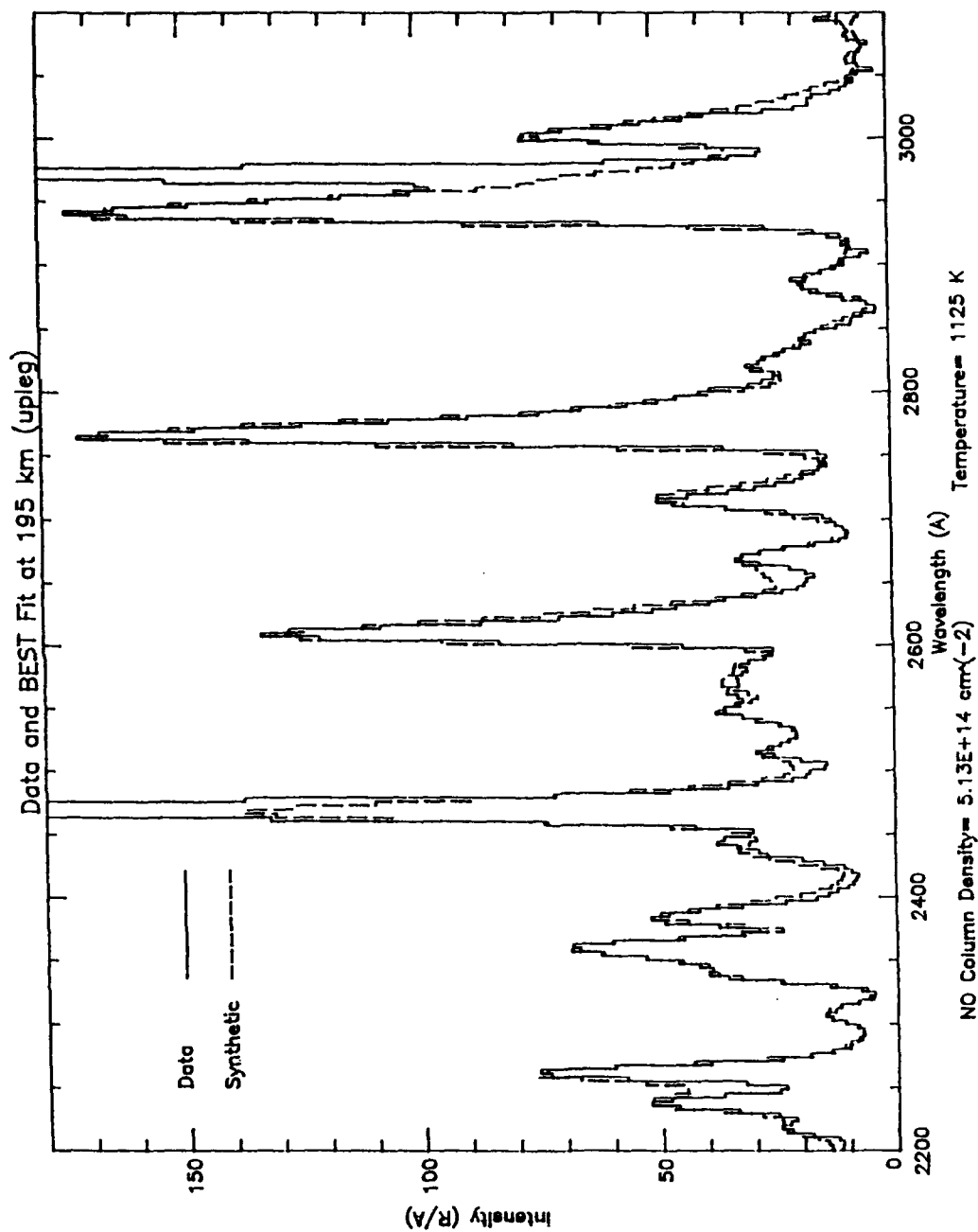
Figure A-21   Comparison of rocket observations at 195km with total synthetic spectrum with minimum scale factors, modified oscillator strengths, and modified Franck-Condon factors applied (Best Fit).

50
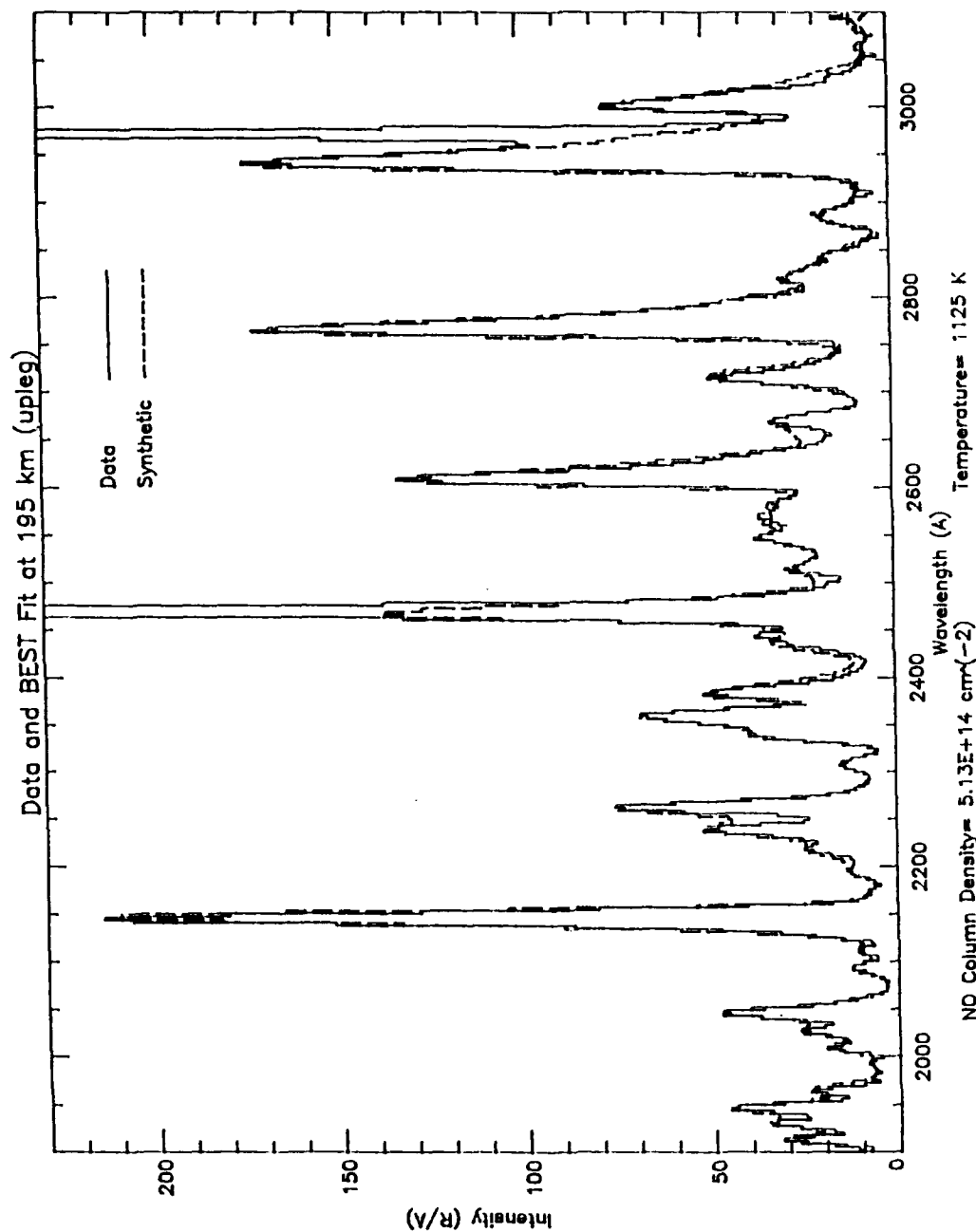
Figure A-22   Comparison of rocket observations at 195km with total synthetic spectrum with minimum scale factors, modified oscillator strengths, and modified Franck-Condon factors applied (Best Fit).
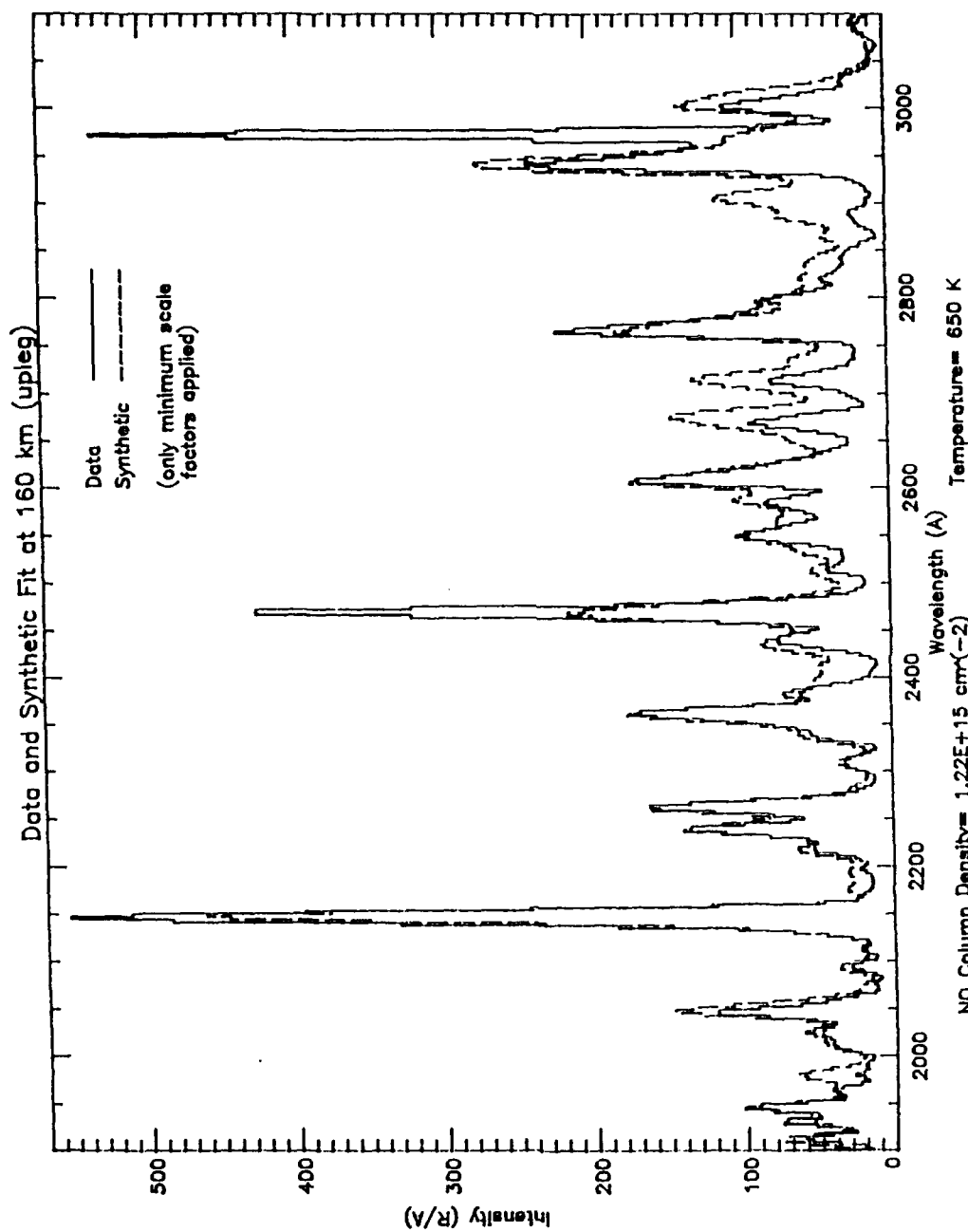
# IX. APPENDIX B

Appendix B contains Figure B-1 which shows the NO column density profile versus altitude and Table B-1 which lists each data point of the NO column density profile as referred to in the results section.

Altitude (km)	NO Column Densities (molecules/cm^2)
100	1.19E+16
105	1.06E+16
110	9.08E+15
115	8.08E+15
120	7.04E+15
125	5.10E+15
130	3.44E+15
135	2.91E+15
140	2.72E+15
145	2.10E+15
150	1.89E+15
155	1.51E+15
160	1.22E+15
165	9.95E+14
170	9.01E+14
175	8.42E+14
180	7.70E+14
185	6.89E+14
190	5.95E+14
195	5.13E+14
200	4.85E+14
205	3.76E+14
210	3.02E+14
215	2.91E+14

Table B-1 NO Column Densities.

Nitric Oxide Column Density (molecules /cm^2)

Altitude (km)

Figure B-1 Nitric oxide column density profile.

X.   APPENDIX C

Appendix C contains Figure C-1 which shows the temperature profile versus altitude and Table C-1 which lists each data point of the temperature profile as referred to in the results section.

54

Altitude (km)	Temperature (K)
100	200
105	200
110	200
115	225
120	225
125	250
130	275
135	350
140	425
145	475
150	625
155	625
160	650
165	675
170	700
175	700
180	750
185	875
190	975
195	1125
200	1200
205	1250
210	1300
215	1375

Table C-1 Temperature vs altitude.
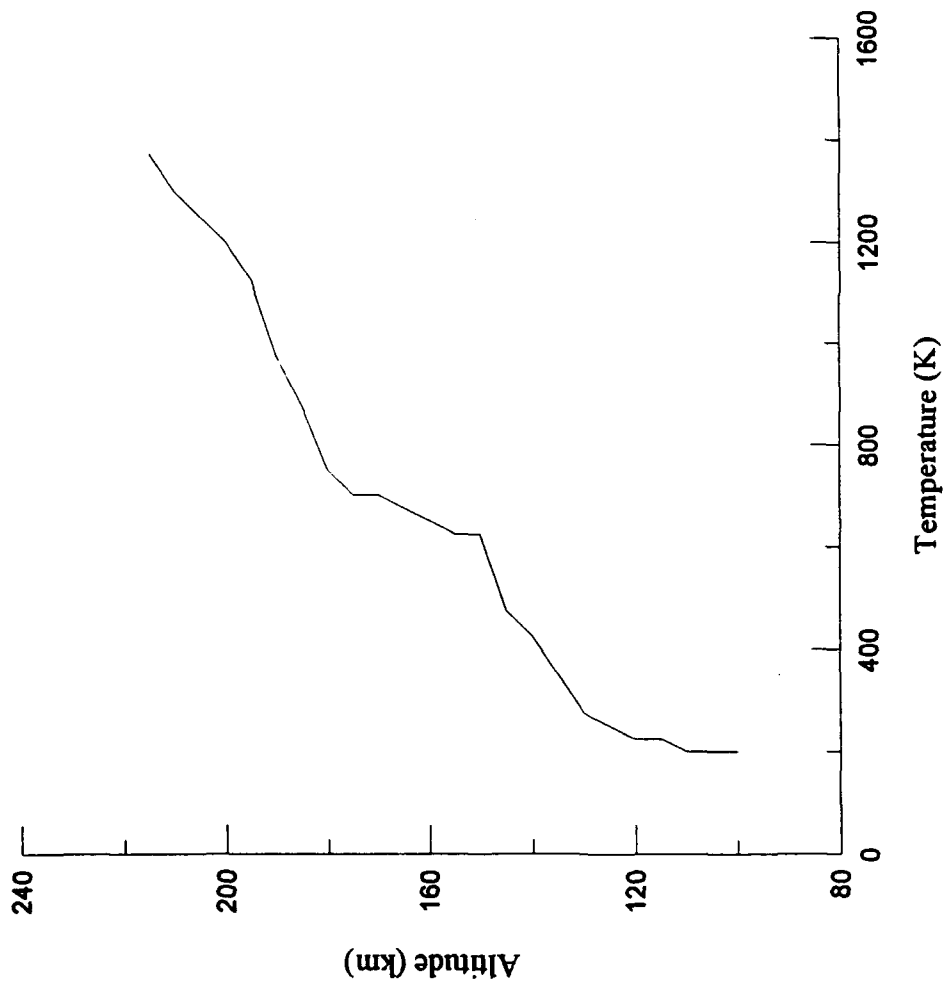
Figure C-1 Temperature profile.

55

XI. APPENDIX D

Appendix D contains the listings for minimum scale factors, modified oscillator strengths, and modified Franck-Condon factors (Best Fits) corresponding to the data bins 110, 160, and 195km. and are shown in Tables D-1 thru D-4.

Table D-1 lists the intensity scale factors for the N_2 LBH and VK synthetic spectra, and the NO γ, δ, and ϵ synthetic spectra.

Tables D-2, D-3, and D-4 contain the fractions necessary to modify each band emission for a best fit. If a fraction is entered for a v' row, it is equivalent to applying that percentage to the molecular oscillator strength. If a fraction is entered for a v" row, it is equivalent to applying that percentage to the molecular oscillator strength and the Franck-Condon factor. If any entry is blank, assume the factor is 1.0.

Table D-1

Synthetic Scale Factors

Altitude (km):	110	160	195
Temperature (Kelvin):	200	650	1125
VK	7.59E+03	1.46E+04	1.59E+04
LBH	4.46E+04	2.50E+04	1.46E+04
NO	3.51E+09	5.46E+08	2.79E+08
NO Column Density:	9.08E+15	1.22E+15	5.13E+14

Synthetic Self Absorption   Scale Factors

0,0	1.00	0.96	0.75
1,0	0.82	0.97	0.72
2,0	0.62	0.48	0.65

Table D-2   Altitude: 110 km   Temp: 200 K

v'	v"	VK	LBH	GAM	EPS	DEL		v'	v"	VK	LBH	GAM	EPS	DEL
0				0.98		0.21		4						
	0					0.12			5	0.45				
	1				0.58	0.12			7	0.32				
	2				0.54				8	0.03				
	3	0.86		0.79	0.62				10	0.32				
	4				0.66				11		0.2			
	5	0.77		0.95					12		0.3			
	6								13		0.3			
	7								14		0.3			
1				0.66					15					
	0			0.83				5						
	1								5					
	2								6					
	3	0.45			0.6				7					
	4			0.74	0.6				8					
	5	0.68							9	0.27				
	6			0.66					10	0.01				
	7	0.55							11					
	8	0.86							12		0.3			
2				0.66					13		0.3			
	0								14		1			
	1			0.74					15					
	2							6			0.23			
	3	0.41							8	0.59				
	4	0.55							9	0.05				
	5	0.14		0.66				7						
	6	0.55							6	0.45				
	7	0.59							10	0.27				
	8	0.55							11	0.01				
	9		0.03					8						
	10		0.03					9						
3				0.5					7	0.68				
	0			0.58					9	0.01				
	1								11	0.01				
	2								12	0.14				
	3							10						
	4								13	0.05				
	5	0.45						12						
	6	0.09							9					
	7								12	0.01				
	8	0.45							14	0.27				
	9							13						
	10		0.04						9	0.45				
	11		0.04						11	0.23				
	12		0.04						13	0.45				

58

Table D-3   Altitude: 160 km   Temp: 650 K

v'	v"	VK	LBH	GAM	EPS	DEL		v'	v"	VK	LBH	GAM	EPS	DEL
0						0.54		4						
	0			0.81		0.38			4	0.74				
	1			0.72	0.86	0.28			5	0.39				
	2				0.46	0.38			7	0.27				
	3	0.66		0.77	0.56				8	0.01				
	4			0.88	0.21				10	0.27				
	5	0.81							11		0.42			
	6	1		0					12		0.86			
	7	0.63							13		0.6			
1									14		0.4			
	0			0.83										
	1			0.77				5						
	2								6	0.39				
	3	0.39		0.71	0.58				9	0.23	0.56			
	4	0.98		0.78	0.42				10	0.01				
	5	0.62		0.79	0.42				12		0.62			
	6			0.75					13					
	7	0.51		0.79				6						
	8	0.56		0.46							0.02			
2			0.1						8	0.51				
	0								9	0.04				
	1							7						
	2			0.58					6	0.39				
	3	0.35		0.52					7	0.55				
	4	0.31							10	0.23				
	5	0.01		0.67					11	0.01				
	6	0.39						8						
	7	0.35							7	0.01				
	8	0.23						9						
	9		0.59						7	0.7				
	10		0.46						9	0.01				
3									11	0.01				
	0								12	0.12				
	1		0.5					10						
	2								13	0.04				
	3							11						
	4								8	0.01				
	5	0.35							10	0.01				
	6	0.08							12	0.04				
	7							12						
	8	0.39							9						
	9								12	0.01				
	10		0.79						14	0.23				
	11		0.7					13						
	12		0.14						9	0.39				
	13								11	0.2				
									13	0.39				

Table D-4   Altitude: 195 km   Temp: 1125 K

v'	v"	VK	LBH	GAM	EPS	DEL	v'	v"	VK	LBH	GAM	EPS	DEL
0				0.53		0.19	4		0.01				
	0			0.71		0.1		4					
	1			0.59	0.48	0.01		5					
	2	0.61			0.06	0.14		7					
	3	0.77		0.42	0.42	0.1		8					
	4	0		0.71	0.42			10					
	5			0.77				11		0.68			
	6							12		0.8			
	7	0.88						13		0.69			
1				0.52				14		0.05			
	0			0.65				15					
	1			0.49			5		0.33				
	2							5	0.01				
	3	0.42			0.06			6	0.09				
	4	0.91		0.58	0.06			7					
	5	0.61		0.58				8					
	6			0.1				9	0.01				
	7	0.53						10	0.01				
	8	0.58						11					
2		0.42		0.52				12		0.76			
	0			0.48				13		0.11			
	1						6		0.28	0.47			
	2			0.45				9	0.01				
	3	0.51					7		0.19				
	4							6	1.03				
	5	0.01						8	0.33				
	6	0.47		0.01				10	0.19				
	7	0.47						11	0.01				
	8	0.79					8		0.28				
	9						9		0.05				
	10		0.8					9	0.01				
3		0.65					10		0.01				
	0							8	0.47				
	1						11		0.14				
	2							8					
	3							10	0.01				
	4							12	0.01				
	5	0.01					12		0.01				
	6	0.19						9					
	7							12					
	8	0.09						14					
	9	0.33					13		0.19				
	10		0.67					9					
	11		0.95					11	0.01				
	12		0.58					13					

60

XII. LIST OF REFERENCES

Anderson, Carl K., *A Calibration of the Naval Postgraduate School Middle Ultraviolet Spectrograph and an Analysis of the OII 2470Å and OI 2972Å Emissions Obtained from Mid-Latitude Rocket Observations*, Master's Thesis, Naval Postgraduate School, Monterey, California, September 1990.

Chase, Bruce E., *A Calibration of the Naval Postgraduate School Middle Ultraviolet Spectrograph (MUSTANG)*, Master's Thesis, Naval Postgraduate School, Monterey, California, December 1992.

Clayton, Michael J., *Analysis of the Ultraviolet Emissions of Nitric Oxide from Mid-Latitude Rocket Observations*, Master's Thesis, Naval Postgraduate School, Monterey, California, June 1990.

Cleary, D.D., "Daytime High-Latitude Rocket Observations of the NO γ, δ, ε Bands," *Journal of Geophysical Research*, v.91, p.11337, 1986.

Eisberg, Robert, and Resnick, Robert, *QUANTUM PHYSICS of Atoms, Molecules, Solids, Nuclei, and Particles*, John Wiley & Sons, 1985.

The Joint Chiefs of Staff Memorandum MJCS Serial 154-86 to Undersecretary of Defense (Research and Engineering), Subject: *Military Requirements for Defense Environmental Satellites*, 01 August 1986.

Mack, Bryan D., *An Analysis of Middle Ultraviolet Emissions of Molecular Nitrogen and Nitric Oxide and Vacuum Calibration of an Ultraviolet Spectrograph*, Master's Thesis, Naval Postgraduate School, Monterey, California, June 1990.

McCoy, R.P., Anderson, D.E., Jr., and Chakrabarti, S., "F2 Region Ion Densities from Analysis of O^+ 834Å Airglow," *Journal of Geophysical Research*, v.90, p.12257, 1985.

Private conversation between D. Cleary, Naval Postgraduate School, and the author, July 1993.

Sharp, William E., *Rocket-Borne Spectroscopic Measurements of the Nirtogen Vegard-Kaplan Bands in the Ultraviolet Aurora*, Ph.D. Dissertation, University of Colorado, 1970.

Walden, Billie S., *An Analysis of Middle Ultraviolet Dayglow Spectra*, Master's Thesis, Naval Postgraduate School, Monterey, California, December 1991.

XIII. BIBLIOGRAPHY

Barth, C.A., Eparvier, F.G., "Self-Absorption Theory Applied to Rocket Measurements of the Nitric Oxide (1,0) Gamma Band in the Daytime Thermosphere," *Journal of Geophysical Research*, v. 97, no. A9, 01 September 1992.

Cleary, D.D., *Analysis of Nitric Oxide Flourescence Bands from High Latitude Rocket Observations of the Thermospheric Dayglow*, Ph.D. Dissertation, University of Colorado, 1985.

Dancyk, Gary Michael, *Identification of Thermospheric Dayglow Emissions for the MUSTANG Experiment*, Master's Thesis, Naval Postgraduate School, Monterey, California, December 1989.

Harrison, George R., and others, *Massachusetts Institute of Technology Wavelength Tables*, John Wiley & Sons, 1960 ed., 1939.

Meier, R. R., "Ultraviolet Spectroscopy and Remote Sensing of the Upper Atmosphere", *Space Science Reviews*, v. 58, nos. 1 & 2, October 1991.

Reader, Joseph, and Corliss, Charles H., *Wavelengths and Transition Probabilities for Atoms and Atomic Ions : Part I. Wavelengths*, National Standards Reference Data System, 1980.

Rees, M.H., *Physics and Chemistry of the Upper Atmosphere*, Cambridge University Press, 1989.

Sharp, William E., and Eastes, Richard W., "Rocket-Borne Spectroscopic Measurements in the Ultraviolet Aurora: The Lyman-Birge-Hopfield Bands," *Journal of Geophysical Research*, v. 92, no. A9, 01 September 1987.

XIV. INITIAL DISTRIBUTION LIST

1. Defense Technical Information Center
    Cameron Station
    Alexandria, Virginia 22304-6145   2

2. Library, Code 052
    Naval Postgraduate School   2
    Monterey, California 93943-5002

3. Dr. William B. Colson, Chairman PH
    Physics Department   1
    Naval Postgraduate School
    Monterey, California 93943-5002

4. Dr. D.D. Cleary
    Physics Department, PH-Cl   3
    Naval Postgraduate School
    Monterey, California 93943-5002

5. Dr. S. Gnanalingam
    Physics Department, PH-Gm   1
    Naval Postgraduate School
    Monterey, California 93943-5002

6. LT Antony C. Marron
    91 Lomitas Road   3
    Danville, California 94526

7. Dr. Robert McCoy
    Code 4140   1
    Naval Research Laboratory
    Washington, D.C. 20375